



Available online at  
**ScienceDirect**  
[www.sciencedirect.com](http://www.sciencedirect.com)

Elsevier Masson France  
**EM|consulte**  
[www.em-consulte.com](http://www.em-consulte.com)



## Original article

First evidence for the early Aptian Oceanic Anoxic Event (OAE1a) from the Western margin of the Pindos Ocean (NW Greece)<sup>☆</sup>Vasileios Karakitsios <sup>a,\*</sup>, Evi Tzortzaki <sup>a</sup>, Fabienne Giraud <sup>b,c</sup>, Nikos Pasadakis <sup>d</sup><sup>a</sup>Department of Historical Geology and Paleontology, Faculty of Geology and Geoenvironment, National and Kapodistrian University of Athens, Panepistimiopolis Zographou, 15784, Athens, Greece<sup>b</sup>University Grenoble Alpes, ISTerre, 38041 Grenoble, France<sup>c</sup>CNRS, ISTerre, 38041 Grenoble, France<sup>d</sup>Hydrocarbons Chemistry and Technology Laboratory, School of Mineral Resources Engineering, Technical University of Crete, 73100 Chania, Greece

## ARTICLE INFO

## Article history:

Received 19 July 2017

Accepted 17 April 2018

Available online 21 April 2018

## Keywords:

Black shales  
 Pindos Ocean  
 Oceanic Anoxic Event  
 OAE 1a  
 Nannofossils  
 Radiolarians  
 Cyanobacterial biomarkers

## ABSTRACT

In this paper, new biostratigraphic, stable isotope (C, O) and organic geochemical data are presented for the Pindos Zone in NW Greece (SE Epirus region) in order to investigate whether the organic carbon rich strata of the Kalarytes sections A and B correspond to a local expression of the early Aptian Oceanic Anoxic Event (OAE 1a or Selli Event) or not. The Pindos Zone Mesozoic to Tertiary sedimentary sequence constitutes the deep-sea sedimentary cover of the Pindos Ocean, which was separated from its oceanic basement as an accretionary prism during the complete closure of this ocean, and was emplaced westwards onto the adjacent Gavrovo-Tripolis carbonate platform. Stable carbon and oxygen isotope data from the Kalarytes sections reveal an isotopic composition compatible with the characteristic features of the OAE 1a. Calcareous nannofossil and radiolarian biostratigraphy indicates an early Aptian age for both sequences. Biomarker analysis on the organic-rich intervals reveals the primary marine origin of the organic matter, with substantial contribution from bacteria, cyanobacteria and dinoflagellates, as well as a significant terrigenous input. Findings of authigenic frambooidal pyrite provide evidence for the prevalence of sulphidic conditions during deposition. Furthermore, similarities between the biomarker signatures of the Pindos organic-rich strata and coeval strata of early Aptian age where the impact of OAE 1a has previously been recorded, are identified. The presented data show that the organic-rich intervals of both Kalarytes sections constitute the first records of the OAE 1a in oceanic deposits of Greece.

© 2018 Elsevier Masson SAS. All rights reserved.

## 1. Introduction

The early Aptian (*ca.* 120 Ma) Oceanic Anoxic Event (OAE 1a or Selli Event) is generally interpreted as a high-productivity event (Coccioni et al., 1992; Erba, 1994, 2004; Erbacher et al., 1996; Cobianchi et al., 1999; Premoli-Silva et al., 1999; Leckie et al., 2002; Aguado et al., 2014; Bottini et al., 2015; Erba et al., 2015) that occurred during a warming interval followed by a cooling trend (Hochuli et al., 1999; Ando et al., 2008; Jenkyns, 2010; Keller et al., 2011; Kuhnt et al., 2011; Najarro et al., 2011; Bottini et al., 2015; Erba et al., 2015; Patruno et al., 2015). It is characterized by a pronounced, abrupt and stepped negative carbon

isotope excursion, recorded in deep- and shallow-marine carbonate containing marine organic matter and terrestrial higher-plant material from Europe, North America, Japan and the Pacific Ocean (Weissert and Lini, 1991; Menegatti et al., 1998; Erba et al., 1999; Gröcke et al., 1999; Jenkyns and Wilson, 1999; Luciani et al., 2001; Ando et al., 2002; Bellanca et al., 2002; Jenkyns, 2003, 2010; Danelian et al., 2004; Luciani et al., 2006; Keller et al., 2011; Bottini et al., 2015; Erba et al., 2015). In pelagic carbonates, the negative shifts to lower  $\delta^{13}\text{C}$  and  $\delta^{18}\text{O}$ -values are synchronous, located just below the black shale that registers the OAE 1a (Bellanca et al., 2002).

OAEs are connected to major perturbations of the global carbon cycle recorded in the isotopic composition of the associated deposits. The early Aptian OAE 1a was interpreted as evidence for the release of  $^{13}\text{C}$ -depleted carbon to the ocean-atmosphere reservoir from either marine volcanism ( $\delta^{13}\text{C} \sim -5\text{\textperthousand}$ ; e.g., Arthur,

<sup>☆</sup> Corresponding editor: Gilles Escarguel.<sup>\*</sup> Corresponding author.E-mail address: [vkarak@geol.uoa.gr](mailto:vkarak@geol.uoa.gr) (V. Karakitsios).

2000) or dissociation of methane gas hydrates ( $\delta^{13}\text{C} \sim -60\text{\textperthousand}$ ; e.g., Jahren et al., 2001; van Breugel et al., 2007). Based on high-resolution C-isotope and biomarker analyses, Méhay et al. (2009) suggested that OAE 1a represents a multi-step C-cycle perturbation triggered by massive volcanism and that a dissociation of  $\text{CH}_4$  gas hydrates, if it existed, was an amplifier and not the cause of the negative C-isotope excursion. Additionally, contrary to the Toarcian OAE, the early Aptian OAE shows relatively less radiometric signatures of the strontium isotope system ( $^{87}\text{Sr}/^{86}\text{Sr}$ ), implying that increased rates of sea-floor spreading and hydrothermal activity dominated over continental weathering in governing sea-water chemistry (Jenkyns, 2003, 2010).

According to Gröcke (2002), the negative carbon-isotope excursion and associated  $\delta^{18}\text{O}$  shift generally took place over a few (tens of) centimeters of sedimentary section, whereas the black shale is typically 1–2 m thick. Such relationships imply paleotemperature change on a time scale of tens of thousands of years. Many authors (e.g., Kuhnt et al., 2011; Huck et al., 2011; Naafs et al., 2016) have attempted to review the duration and chronology of OAE 1a and determined more accurately the relative timing of the associated events using various paleo-proxies. Kuhnt et al. (2011) presented bulk rock carbon and oxygen isotope data from La Bédoule (southeast France), which reveals that the negative carbon isotope excursion preceding OAE 1a lasted more than 100 kyr. According to these authors, the main positive carbon isotope shift at the onset of OAE 1a, previously regarded as continuous, occurred stepwise over a period of > 300 kyr. Huck et al. (2011) reported carbon and strontium isotope chronostratigraphic data from the Barremian-Aptian Urgonian carbonate platform (Subalpine Chains, Haute-Savoie, ESE France) indicating that carbonate production in this platform ceased about 300 kyr before the most negative values of the carbon-isotope excursion, which marks the beginning of OAE 1a. Naafs et al. (2016) provided a high-resolution record of  $\text{pCO}_2$  across OAE 1a from an expanded section in Southern Spain and Tunisia and found that atmospheric  $\text{CO}_2$  concentrations increased significantly during this anoxic event and remained above background values for approximately 1.5 to 2 myr before declining. The period of elevated  $\text{CO}_2$  concentrations coincides with a shift in the oceanic osmium-isotope record.

$\text{TEX}_{86}$  data obtained from the organic matter in the tropical Pacific ODP site 1207, show warmer temperatures associated with the OAE 1a (up to 36 °C for sea surface), but with many fluctuations ( $\pm 7$  °C around this value) associated with the event (Dumitrescu et al., 2006). Other  $\text{TEX}_{86}$  data carried out on a section of the Lower Saxony Basin show a warming in high latitudes during the OAE 1a (Mutterlose et al., 2010). More recently, high-resolution  $\delta^{18}\text{O}_{\text{carb}}$  data obtained on the Gare de Cassis-La Bédoule section (Provencal Basin, south France) by Kuhnt et al. (2011) illustrate a cooling of 3–5 °C in the lower part of the OAE 1a (C4 isotopic segment). Based on calcareous nannofossil, Bottini et al. (2015) oxygen isotope and  $\text{TEX}_{86}$  data from the Cismon and Piobbico cores (Tethys) and DSDP Site 463 (Pacific Ocean) suggested that the Ontong Java Plateau (OJP) volcanic activity caused global warming whereas other mechanisms (weathering, deposition of organic matter) acted as feedback processes, favouring “cold snaps” during the early Aptian. Naafs and Pancost (2016) presented high-resolution  $\text{TEX}_{86}$ -based records of the Sea Surface Temperatures (SST) during OAE 1a from the DSDP Site 398, located in the proto-North Atlantic. Their results demonstrate that changes in SSTs (increase by ~2–4 °C during OAE 1a, and decrease by ~4–6 °C at its end) coincided with changes in  $\delta^{13}\text{C}_{\text{org}}$ -values presumably due to light organic carbon release resulting in  $\text{pCO}_2$ -forced global warming, followed by organic matter sequestration and  $\text{pCO}_2$ -forced cooling.

Detailed  $^{187}\text{Os}/^{188}\text{Os}$  profiles through the Livello Selli in Italy show an early pulse of radiogenic osmium to the oceans interrupting a trend toward lower values due to submarine

volcanism and attendant hydrothermal activity as in the case of the OAE 2 event (Bonarelli event; Tejada et al., 2009; Jenkyns, 2010). Bottini et al. (2012) used Rhenium-Osmium isotope data from two sites in the Tethys and Pacific Oceans to confirm the relationship between the sequence of volcanic activity of the OJP, the accumulation of  $\text{CO}_2$  in the ocean-atmosphere system, and the OAE 1a during the latest Barremian–early Aptian. Their data provide evidence for at least two major volcanic phases during this time interval.

Erba et al. (2015) presented new data from DSDP (Magellan Rise and Mid-Pacific Mountains), ODP (Resolution Guyot), and Cismon and Piobbico drill sites to explore the association between submarine volcanism and OAE 1a. The early Aptian paleoecosystem responses to volcanic activity include the stimulation of marine phytoplanktonic populations and the temporary decline of many calcifying marine organisms which were forced to adapt and survive under eutrophic conditions and/or toxic waters. Nannoplankton and benthic communities recovered after the end of the massive volcanic activity with an evolutionary radiation as a strategic response. According to Erba et al. (2015), the major early Aptian magmatic event did not trigger extinctions of oceanic biota.

In this paper, new biostratigraphic, chemostratigraphic and organic geochemical data are presented from black shale horizons contained in the deep-sea deposits of the Pindos Zone, Northwestern Greece. These horizons are cropping out within the Aptian-Albian sequences of the Kalarrytes sections A and B (Epirus region, NW Greece). In the context of global-scale OAEs, these new observations and results provide insights into the paleoenvironmental conditions prevailing along the western margin of the Pindos Ocean during the early Aptian and the biotic response to prolonged periods of oceanic anoxia.

## 2. Geological setting and paleogeographic framework

The Pindos Zone (Fig. 1) comprises an intricate thrust belt with allochthonous Mesozoic to Tertiary sedimentary rocks of deep-water facies. The zone extends into Albania and the former Yugoslavia (Dédé et al., 1976; Robertson and Karamata, 1994) as well as into Crete (Bonneau, 1984), Rhodes (Aubouin et al., 1976), and Turkey (Bernoulli et al., 1974; Argyriadis et al., 1980). The Pindos Zone sequence originated from an elongate remnant ocean basin that formed in mid-Triassic times along the north-eastern passive margin of Apulia, between the extensive Gavrovo-Tripolis platform which was periodically emerged (Fleury, 1980), in the present west, and the Pelagonian continental block in the east (including also the isolated Parnassos Platform in its western portion).

Observations on the Greek mainland, as well as on the island of Crete, confirm that the eastern basal rocks of the Pindos Zone and the south-western end of the Pelagonian continental terrain were rifted from Gondwana in mid-Triassic times (De Wever, 1976; Bonneau, 1982; Clift, 1992; Degnan and Robertson, 1998; Pe-Piper, 1998). By Early Jurassic times at the latest, actively spreading oceanic basins opened in both the Pindos and the Vardar zones on both sides of the Pelagonian continental block. The western, Pindos Ocean separated Pelagonia from Apulia; the eastern, Vardar Ocean separated Pelagonia from the Serbomacedonia and Sakarya microcontinents (De Wever, 1976; Bonneau, 1982, 1984; Clift, 1992; Lefèvre et al., 1993; Pe-Piper and Hatzipanagiotou, 1993; Degnan and Robertson, 1998; Pe-Piper, 1998). Significant data supporting the oceanic nature of the Pindos Basin are given by Degnan and Robertson (1998), and Palamakumbura et al. (2013).

The later Mesozoic and Cenozoic convergence resulted in the nappe structure of the Hellenide Orogen and the tectonic dismemberment of the Permian-Triassic rift-related igneous

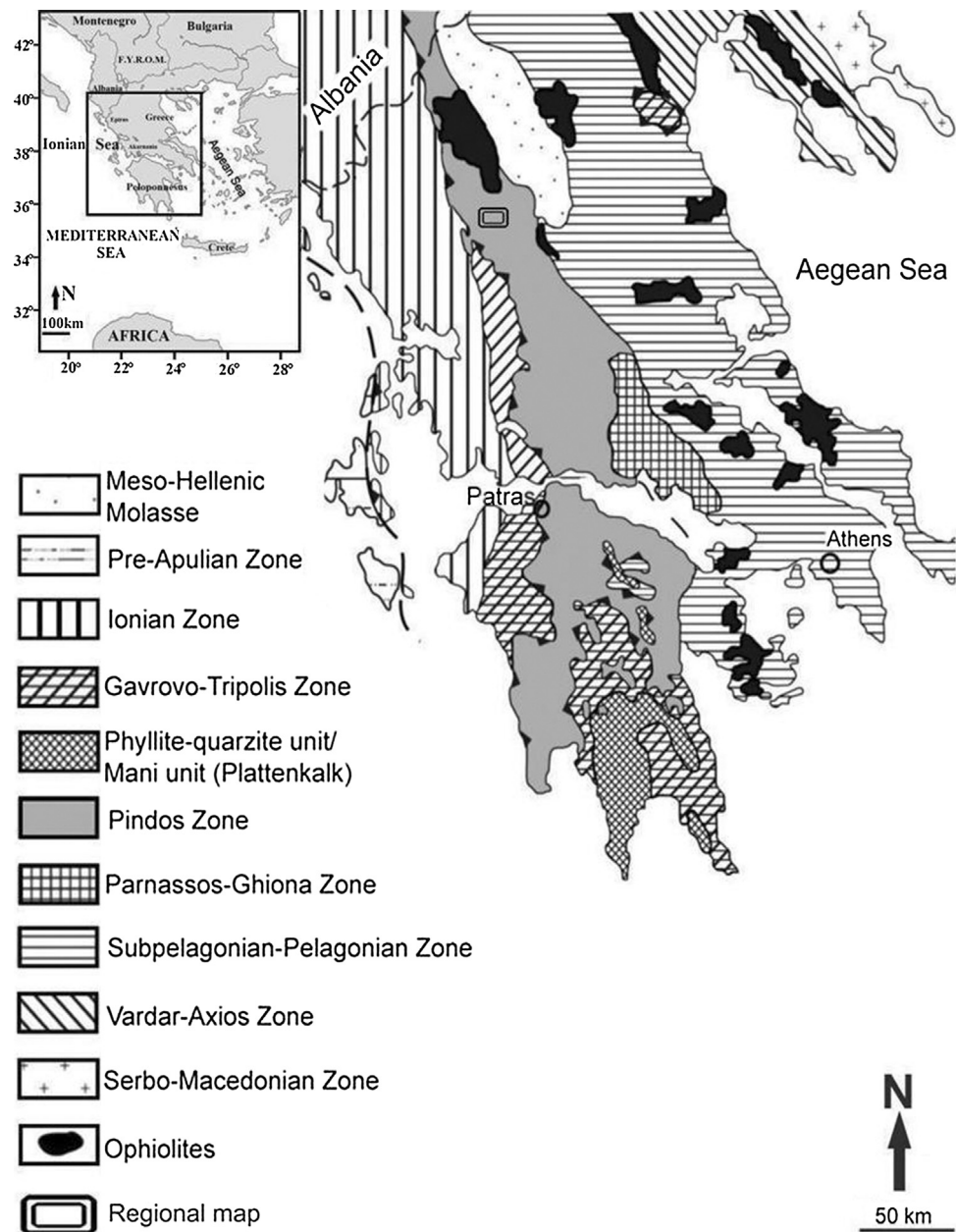


**Fig. 1.** Simplified geological map of Greece. Top-left inset provides the geographical location of the regional Kalarytes map.

rocks. The subsequent collision of the Apulian and Pelagonian continents was characterized by detachment of the Pindos Ocean's western margin deep-sea deposits (Pindos Zone) and their incorporation into a west-vergent subduction-accretion complex, which is well exposed in the Greek mainland and Crete. The Pindos Zone of Western Greece is exceptional since it was deformed into a regular series of thrust sheets during its emplacement, with a minimum of disruption. The present-day westward-vergent fold and thrust sheets have not been affected by major back-thrusting or out-of-sequence thrusting (Degnan and Robertson, 1998).

The sedimentary successions of the Pindos Zone comprise deep-water carbonate, siliciclastic and siliceous rocks ranging in age from Late Triassic to Eocene (Fleury, 1980; Degnan and Robertson, 1998; Figs. 2, 3). The oldest rocks (of Carnian age) comprise disrupted siliciclastic turbidites largely derived from a metamorphic source to the west and deposited on young oceanic basement. Variable thicknesses of pelagic carbonates and cherts, marls and proximal carbonate debris flows accumulated from the Norian to

the Maastrichtian, while radiolarites *sensu stricto* are mainly observed in the Aalenian to Tithonian interval.

During the Early and early Late Cretaceous, paleogeographic conditions (Figs. 3, 4) favored the deposition of abundant radiolarites *sensu lato* (Red marls; Fleury, 1980), in which organic-rich horizons have been observed (Neumann and Zacher, 2004; Karakitsios et al., 2006; Karakitsios and Agiadi-Katsiaouni, 2007). The above sequence is followed by pelagic and turbiditic limestone deposits in the higher Upper Cretaceous (Platy limestone; Fleury, 1980; Neumann and Zacher, 2004; Karakitsios et al., 2006). From the end of the Maastrichtian onwards, a progressive closure of the Pindos oceanic basin is recorded by a gradual change in sedimentary rock composition (late Maastrichtian transitional formation "couches de passage") from dominantly carbonate deposition to siliciclastic turbidites (Paleocene flysch deposition) derived from the north and east sectors (Fleury, 1980; Neumann and Zacher, 2004). During the Eocene, the complete closure of the Pindos Ocean resulted in the detachment of its

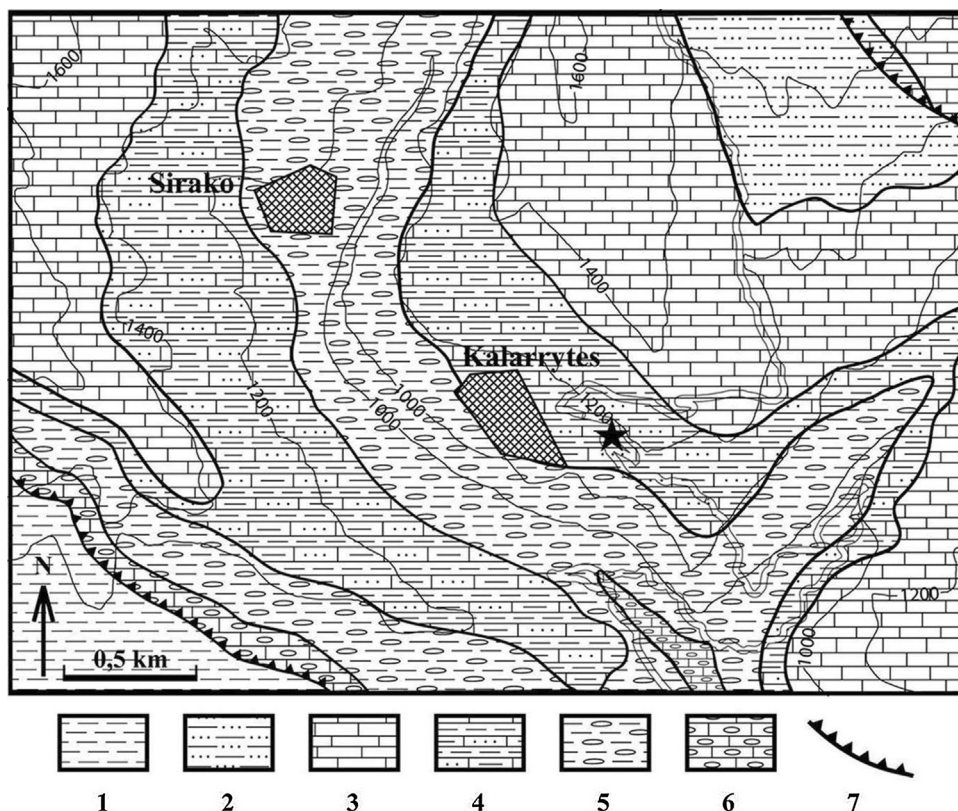


**Fig. 2.** Regional geological map of Kalarytes: Ionian zone: 1, Flysch. Pindos zone: 2, flysch; 3, Platy limestones (Upper Cretaceous); 4, Limestone, marl and chert beds alternations (Barremian-Albian); 5, Radiolarites s.l. (Toarcian-Hauterivian); 6, Limestone and jasper alternations; 7, Thrust. The asterisk shows the position of the study area.

deep-sea sedimentary cover from its oceanic basement as an accretionary prism and emplacement westwards onto the adjacent Gavrovo-Tripolis carbonate platform, ending up as a series of thin-skinned thrust sheets.

### 3. The Kalarytes sections

#### 3.1. Section A

This section is located (asterisk in Fig. 2) about 20 m east of the first bend of the Ioannina-Kalarytes road (close to the topographic low of Kalarytes village; 39°34'59.60"N, 21°07'36.30"E). The upper 8 m of the section are observed above the road level, while the lower 7 m are observed below it (Fig. 5). There is an observation gap of 3 m between the two parts. In this area, and generally in the Epirus region (NW Greece), the Pindos Zone directly overthrusts the Ionian Zone, having tectonically superimposed the entire Gavrovo-Tripolis Platform. Consequently, the observed outcrops, which are located in the westernmost part of the Pindos Zone, were located in paleogeographic vicinity with the adjacent Gavrovo-Tripolis carbonate platform. Since the section corresponds to the reversed limb of a decametric fold, it will be described in its normal position. Therefore, from the original bottom to top, it contains (Figs. 3, 5):

- 2 m of pelagic limestone beds with cherty nodules, interbedded with rare centimeter- to decimeter-thick radiolarian chert beds;
- 3 m of laminated marls and claystones with rare intercalations of chert beds, marly limestones and pelagic limestones with cherty nodules. In the base of the upper part of this interval, a 1 m-thick black shale horizon is observed, which mainly consists of laminated marls;
- 3 m of pelagic limestone beds with the same characteristics as the first 2 m of the section (with cherty nodules, interbedded

with rare cm- to dm-thick radiolarian chert and pelagic limestone beds);

- 6 m, above the observation gap, the outcrop continues with the same lithology.

#### 3.2. Section B

This section (39°34'43.73"N, 21°08'01.38"E) is located about 800 m southeast of the section A (asterisk in Fig. 2). From bottom to top (Figs. 3, 6) are observed:

- 4 m beginning by marly limestone, followed by laminated marls with rare cherty beds intercalations;
- 15 cm-thick black shale horizon;
- 1 m of marls alternating with pelagic cherty limestones and cherty beds.

### 4. Material and methods

#### 4.1. Sampling

Twenty-six samples were collected from section A, 15 of which were taken exclusively from the 3 m-thick bed of laminated marls and claystones containing the black shale horizon (Fig. 3). Forty-two samples were collected from section B, 35 of which were taken from the upper 2 m of the section (every 5–10 cm) where the organic-rich bed is observed.

#### 4.2. Bulk organic geochemistry

Geochemical analysis was carried out in the "Hydrocarbons Chemistry and Technology" Research Laboratory, School of

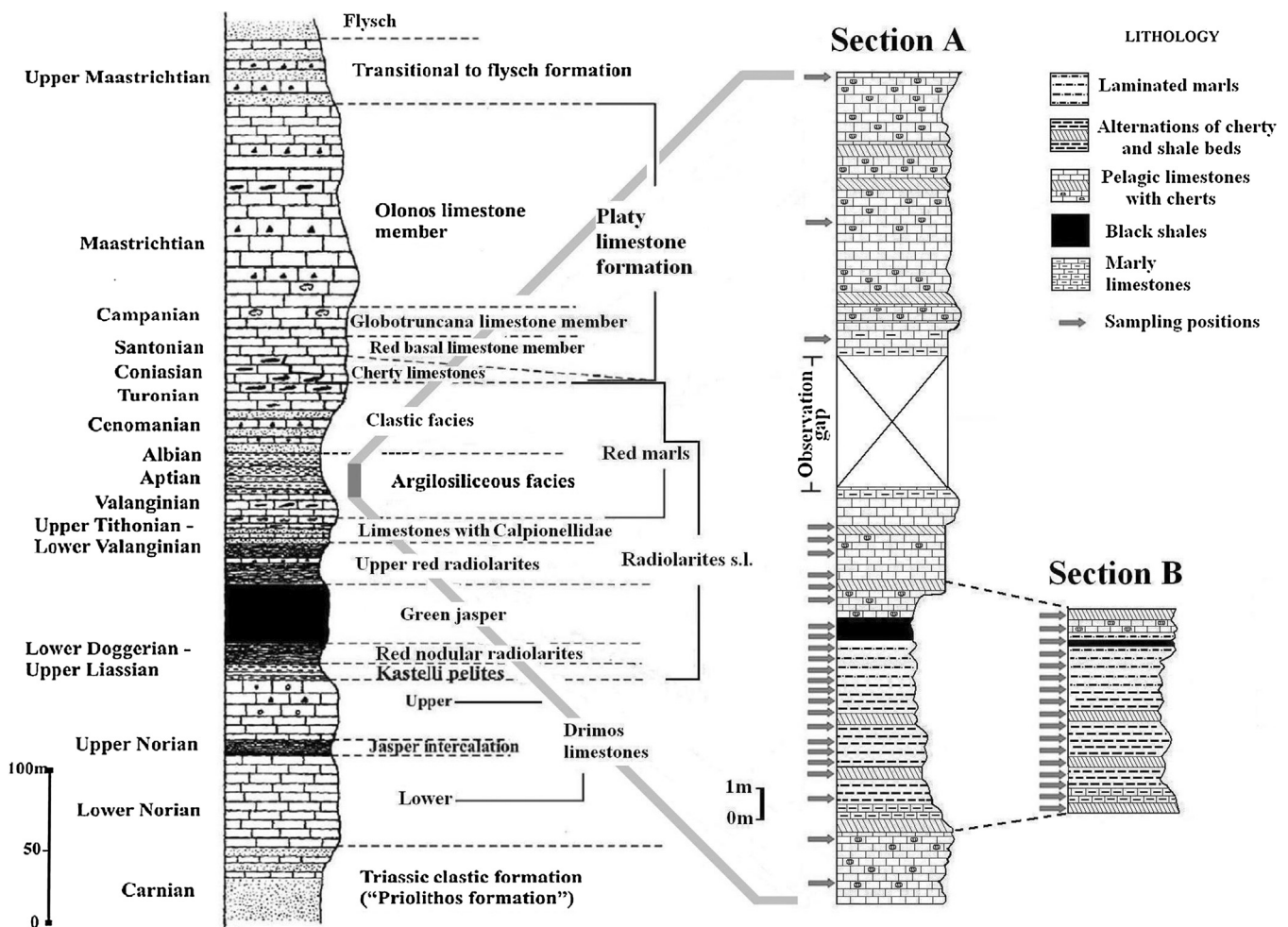


**Fig. 3.** Left: Synthetic stratigraphic column of the Pindos zone (after Karakitsios et al., 2007, modified). Right: Stratigraphic columns of the Kalarytes sections A and B.

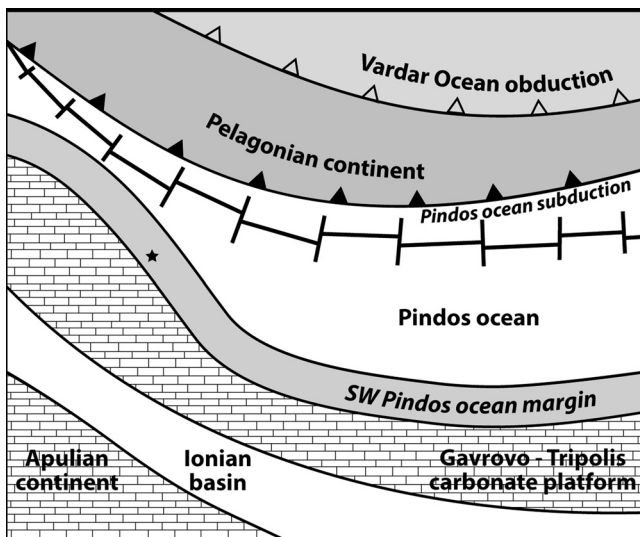


**Fig. 4.** Schematic paleogeographic reconstruction of the Pindos Ocean during the early Aptian (Lower Cretaceous). The asterisk shows the position of the study area.

Mineral Resources Engineering, Technical University of Crete. All 68 rock samples of both sections, dried at 40 °C overnight, were powdered using an agate mortar. Aliquots of the powdered samples (~100 mg) were analyzed in a Rock-Eval RE II-TOC (Delsi Inc.) system connected to an SRI-302 A/D data acquisition system.

After a 2 min purging with He, the samples were heated at 300 °C for 3 min and afterwards were pyrolyzed up to 600 °C, following a temperature ramp equal to 50 °C·min<sup>-1</sup>. The CO<sub>2</sub> trap was functioning until 390 °C. The pyrolyzed rock samples were further burned in the oxidation oven at 600 °C. Total organic carbon (TOC) of the samples was calculated based on the RE experimental data using the PeakSimple 3.29 software. Quantification was based on calibration data from standard rock samples (Tables S1, S2; Appendix A). Determination of calcium carbonate content of the samples was carried out in the Laboratory of the Department of Historical Geology and Paleontology, National and Kapodistrian University of Athens applying the method of "carbonate bomb" (Müller and Gastner, 1971) (Tables S1, S2; Appendix A).

#### 4.3. Stable carbon and oxygen isotopes

Twelve dried and powdered rock samples from section A (ca. 10 mg each) were analyzed for carbonate carbon and oxygen isotope ratios at the Stable Isotope Unit of "Demokritos" National Center of Scientific Research, Department of Material Science, Athens (accredited by ISO 17025: 2005, Certificate Number 579). Samples with a carbonate content lower than 10% w/w were not analyzed for their carbonate isotope ratios because the results would not be reliable (Table S1, Appendix A).

Carbonate isotope ratios (<sup>13</sup>C/<sup>12</sup>C and <sup>18</sup>O/<sup>16</sup>O) were measured on a Thermo Delta V Plus Isotope Ratio Mass Spectrometer equipped with a GasBench II device. Isotope ratios were determined on CO<sub>2</sub> gas yielded after reaction with orthophosphoric acid

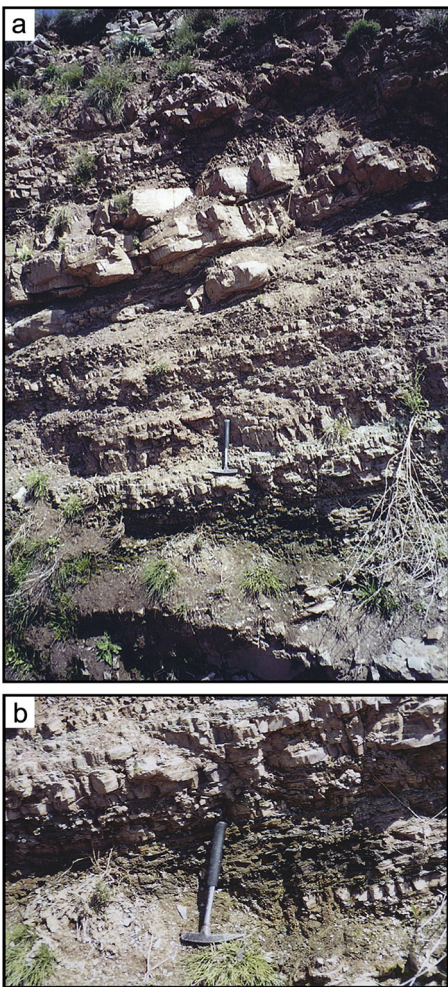


**Fig. 5.** Views of the Kalarytes section A. **a.** Early Aptian laminated marls and claystones with rare chert bed intercalations; organic-rich horizon below the hummer. **b.** Detail of the organic-rich horizon shown in (a).

( $\text{H}_3\text{PO}_4$ ) at 72 °C (Table S1). Normal corrections were applied and the analytical results are reported in the usual  $\delta$ -notation, in ‰ deviation from the V-PDB (Vienna Pee Dee Belemnite) standard. Calibration to VPDB was performed against NBS 18 and NBS 19 carbonates and an internal Carrara marble standard. Reproducibility of replicate analyses of standards was generally better than 0.05‰ for both carbon- and oxygen-isotope ratios (analytical error for isotopic analyses  $\delta^{13}\text{C}$  and  $\delta^{18}\text{O}$  less than 0.05‰).

Thirty samples from the section B were analyzed at the laboratory of Biominerizations and Sedimentary environments (Pierre and Marie Curie University; Paris 6). The measurements on the bulk samples were conducted with a mass spectrometer VG SIRA 9. The  $\text{CO}_2$  extraction was attained through reaction of powder samples (50–100 mg) with anhydrous orthophosphoric acid at 50 °C. Resulting values were expressed in per mil relative to the V-PDB standard reference (Table S2).

#### 4.4. Biostratigraphic analysis

##### 4.4.1. Calcareous nannofossils

Twenty-six samples from section A, the same as for bulk organic geochemistry, were investigated for calcareous nannofossil semi-quantitative analyses. Smear slides were prepared as homogeneously as possible and no ultrasonic cleaning or centrifuge concentration was applied in order to retain the original biogenic composition of samples. The investigation was restricted to

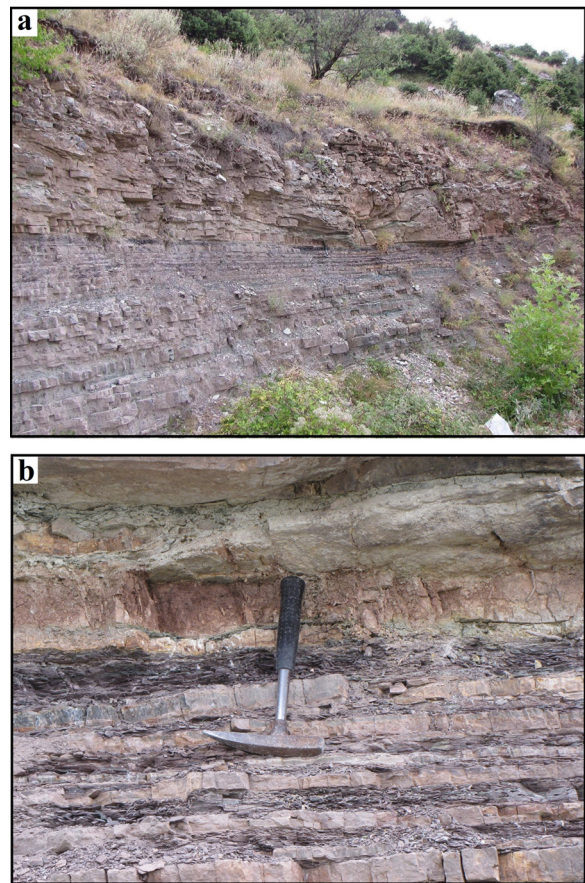


**Fig. 6.** Views of the Kalarytes section B. **a.** Organic-rich horizon (below the hummer, used as a scale). **b.** Detail of the organic-rich horizon shown in (a).

biostratigraphic markers observed under a light polarizing microscope with a magnification of  $\times 1000$ , following different transverse sections (up to 20 in the richest sample; Fig. 7). The taxonomic framework of Bown et al. (1998) was used. For nannoconids, and for both *Assipetra* and *Rucinolithus* genera, those of Deres and Achéritéguy (1980) and Tremolada and Erba (2002) were followed, respectively.

The nannofossil preservation was evaluated following the classes defined by Roth (1983). Abundance terminology used in this study refers to those defined by Lozar and Tremolada (2003). The nannofossil biostratigraphic zones and subzones applied to the investigated section are the NC zones of Bralower et al. (1993, 1995), modified from Roth (1978). This zonation scheme has been selected because of its applicability to both pelagic deposits and low-latitude Tethyan continental margins (Bralower et al., 1993). The smear slides prepared for calcareous nannofossil biostratigraphic analyses were observed under a light polarizing microscope (magnifications  $\times 100$  and  $\times 200$ ) to investigate the presence of pyrite.

##### 4.4.2. Radiolarian

Three samples from section A (7KA, 10KA, 11KA) and nine samples from section B (8KB, 11KB, 18KB, 21KB, 24KB, 32KB, 36KB, 38KB, 41KB) were investigated for radiolarian assemblages. The samples from section A were crushed into small fragments (*ca.* 2 cm) and soaked in dilute hydrochloric acid (8% w/w) for *ca.* 16 hours whereas the samples from section B were soaked in hydrochloric acid 4% w/w for 24 hours. The samples were rinsed with distilled water and dried in a temperature of 60 °C. Radiolarians were observed under a stereoscopic microscope,

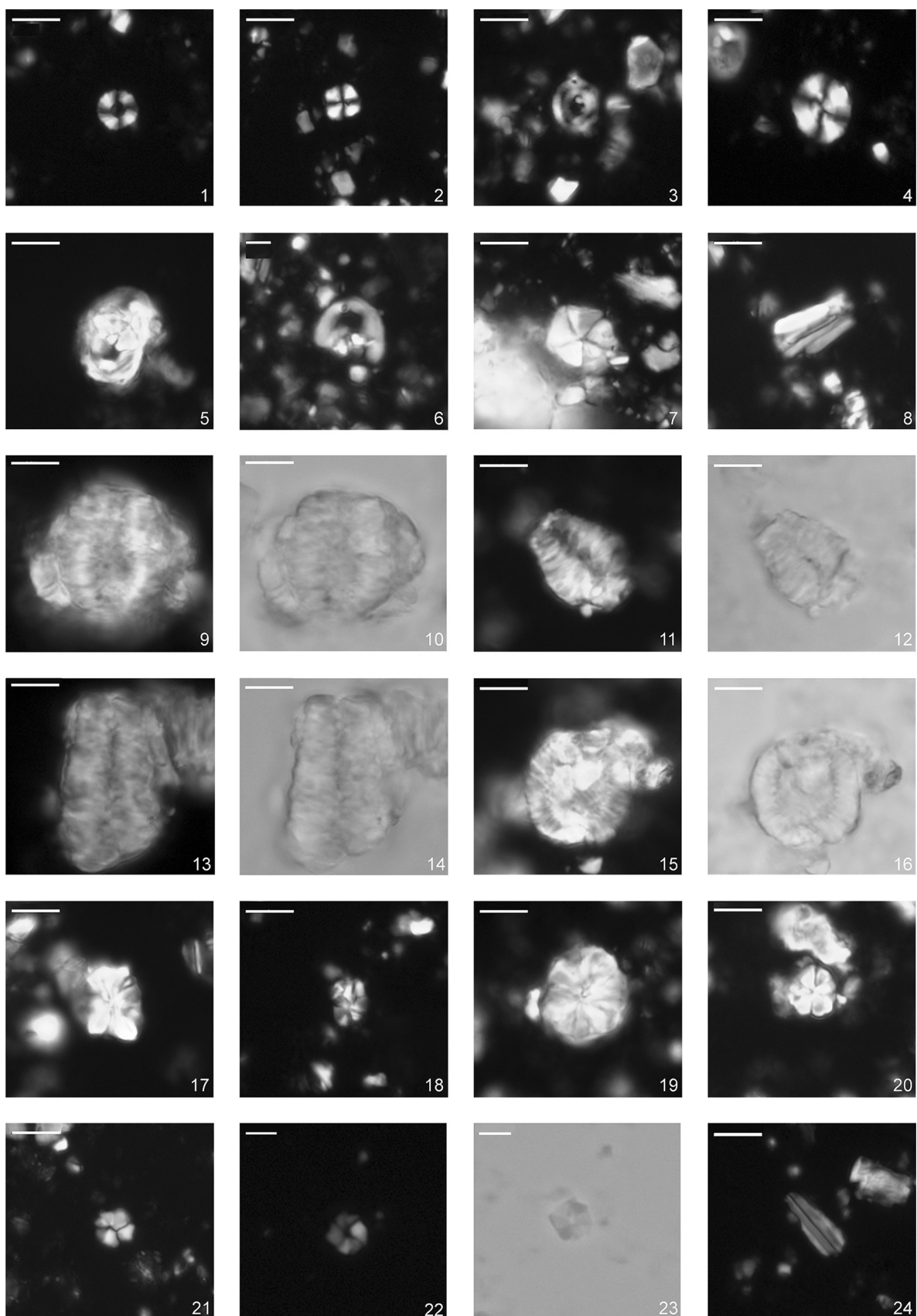


**Fig. 7.** Light microscope pictures of selected calcareous nannofossil species from the Kalarytes section A. **1.** *Diazomatolithus lehmanni* Noël, 1965; sample 1KA. **2.** *Cyclagelosphaera margerelli* Noël, 1965; sample 4KA. **3.** *Helenea chiastia* Worsley, 1971; sample 25KA. **4.** *Watznaueria barnesiae* (Black, 1959) Perch-Nielsen, 1968; sample 4KA. **5.** *Zeugrhabdotus embergeri* (Noël, 1958) Perch-Nielsen, 1984; sample 1KA. **6.** *Zeugrhabdotus scutula* (*Bergen*, 1994) Rutledge et Bown, 1996; sample 1KA. **7.** *Micrancolithus hoschulzii* (Reinhardt, 1966) Thierstein, 1971; sample 6KA. **8.** *Conosphera mexicana* subsp. *mexicana* Trejo, 1969; sample 1KA. **9, 10.** *Nannoconus kampptneri* subsp. *kampptneri* Bronnimann, 1955; sample 1KA. **11, 12.** *Nannoconus steinmannii* subsp. *minor* Kampptner, 1931; sample 4KA. **13, 14.** *Nannoconus steinmannii* subsp. *steinmannii* (Kempf, 1931) Kampptner, 1931; sample 1KA. **15.** *Nannoconus steinmannii* subsp. *steinmannii* (Kempf, 1931) Kampptner, 1931; sample 1KA. **16.** *Nannoconus steinmannii* subsp. *steinmannii* (Kempf, 1931) Kampptner, 1931; sample 1KA. **17.** *Nannoconus steinmannii* subsp. *steinmannii* (Kempf, 1931) Kampptner, 1931; sample 1KA. **18.** *Nannoconus steinmannii* subsp. *steinmannii* (Kempf, 1931) Kampptner, 1931; sample 1KA. **19.** *Nannoconus steinmannii* subsp. *steinmannii* (Kempf, 1931) Kampptner, 1931; sample 1KA. **20.** *Nannoconus steinmannii* subsp. *steinmannii* (Kempf, 1931) Kampptner, 1931; sample 1KA. **21.** *Nannoconus steinmannii* subsp. *steinmannii* (Kempf, 1931) Kampptner, 1931; sample 1KA. **22.** *Nannoconus steinmannii* subsp. *steinmannii* (Kempf, 1931) Kampptner, 1931; sample 1KA. **23.** *Nannoconus steinmannii* subsp. *steinmannii* (Kempf, 1931) Kampptner, 1931; sample 1KA. **24.** *Nannoconus steinmannii* subsp. *steinmannii* (Kempf, 1931) Kampptner, 1931; sample 1KA.

picked using a trimmed paint brush, and transferred temporarily to microslides for qualitative analysis.

#### 4.5. Biomarker analysis

Seven samples from section A and one sample from section B were selected for detailed investigation of the contained biomarkers, based on their stratigraphic level and their TOC content. The analysis was carried out using gas chromatography–mass spectrometry (GC–MS) in the “Hydrocarbons Chemistry and Technology” Research Laboratory, School of Mineral Resources Engineering, Technical University of Crete. An experimental protocol of extraction, desulfurization and extract fractionation was applied as a preparatory scheme for the subsequent GC–MS analysis. The seven samples from section A were extracted ultrasonically. A three-solvent extraction scheme was followed (Hopmans et al., 2000). In the sample from section B, the Soxhlet extraction technique was applied for 24 hours using dichloromethane (DCM) as solvent. The amounts of the obtained total lipid extract (TLE) of each sample and the relative amounts of the extractable organic matter are shown in Table S3 (Appendix A). The total lipid extracts were treated with acid-activated copper to remove elemental sulfur, following the procedure described by Forster et al. (2004).

Column chromatography was used for the initial separation of the rock extracts into fractions of increasing polarity. Three fractions were collected by sequential elution with the following solvents:

- n-hexane to elute aliphatic compounds;
- DCM: n-hexane (1:1 vol.) to elute aromatic compounds;
- DCM for the polar compounds.

The GC–MS analysis was carried out on an Agilent 7890A gas chromatograph coupled to an Agilent 5975E mass spectrometer with an automatic liquid sampler (ALS).

For the analysis of the seven samples from the Kalarytes section A, the GC was equipped with an electronic program controlled (EPC) split-splitless injector and an Agilent capillary column DB-5MS UI (30 m × 250 µm × 0.25 µm). Helium was used as the carrier gas. The oven temperature was programmed at 40 °C for 2 min, followed by a 20 °C·min<sup>-1</sup> ramp to 200 °C, a second 2 °C·min<sup>-1</sup> ramp up to 300 °C, and a final isothermal time of 20 min. The transfer line was set at 280 °C, and the MS source was set at 230 °C. The injected volume was 0.5 µl, and the total run time was 80 min. Six different internal standards were added prior to GC–MS analysis to the aliphatic and the aromatic fractions. The electron impact (EI)-mass spectra were acquired at 70 eV in full scan mode (scan range from *m/z* = 50 to 550). Data were acquired and processed under HP mS-ChemStation software. Compounds were identified by their relative retention times and by comparison with mass spectra reported in the literature.

For the analysis of the sample from section B, a different capillary column was used (HP-5MS UI, 60 m × 250 µm × 0.25 µm). The oven temperature was programmed at 40 °C for 2 min, followed by a 20 °C·min<sup>-1</sup> ramp up to 200 °C, a second 2 °C·min<sup>-1</sup> ramp up to 300 °C, and a final isothermal time of 60 min. The transfer line was set at 280 °C, and the MS source was set at 230 °C. The injected volume was 0.5 µl, and the total run time was 120 min.

#### 4.6. Scanning Electron Microscopy (SEM)

From the microslides (see Section 4.4.2), selected well-preserved radiolarian specimens from both sections were transferred to copper SEM stubs, attached by means of a double-faced adhesive tape, and coated with gold. A scanning electron microscope JEOL JSM-6390 (Department of Historical Geology and Paleontology, University of Athens) was used for SEM observations and photographs of the specimens.

#### 4.7. Repository

The slides prepared for the analyses of calcareous nannofossil biostratigraphy and pyrite distribution of the Kalarytes section A are deposited in the Laboratory of the Department of Historical Geology and Paleontology, National and Kapodistrian University of Athens, with the curatorial numbers 1KA2014–26KA2014. The thin sections and fossil radiolarian specimens prepared for SEM analyses are deposited in the same Laboratory with the additional numbers 7KATS301015 and SEMRAD1015A–SEMRAD1015B, respectively. For the biostratigraphic analysis of the Kalarytes section B, fossil radiolarian specimens prepared for SEM analyses are deposited in the same Laboratory with the numbers SEMRAD1702168KB, SEMRAD17021611KB, SEMRAD17021618KB, SEMRAD170216321KB, SEMRAD170216324KB, SEMRAD17021632KB, SEMRAD17021636KB, SEMRAD17021638KB, and SEMRAD170216341KB.

### 5. Results

#### 5.1. Biostratigraphy

##### 5.1.1. Calcareous nannofossils

All the nannofossil taxa observed in the Kalarytes section (Fig. 7) are reported in a distribution chart (Fig. 8). Of the 26 samples, 20 are barren of nannofossils, 2 present traces of nannofossils with only 1 or 2 species identified, and 4 present rare to few nannofossils (1KA, 4KA, 6KA, 25KA). In the latter 4 samples, the preservation is poor with strongly etched and moderately overgrown specimens. Overall, thirty-three species have been recognized. The assemblages are similar and characterized by age-diagnostic taxa; sample 1KA exhibits the highest species richness. In the four samples, the nannofossil assemblages are dominated by *Watznaueria barnesiae*. In sample 1KA, other common taxa are the group of *Nannoconus*, especially *N. steinmannii* (both subspecies *minor* and *steinmannii*), and the group of *Assipetra infracretacea* (common small- and rare large-sized) and *Reticulolithus terebrodentarius* (medium- and large-sized); frequent species are *Watznaueria fossacincta*, *W. manivitiae*, *Cyclagelosphaera margerelii*, *Zeugrhabdotus embergeri*, *Lithraphidites carniolensis*, and small specimens of *Helenea chiastra*. In sample 4KA, nannofossils are rare, essentially represented by *W. barnesiae*, then by *W. fossacincta*, *Nannoconus* spp. and the group of *Assipetra* + *Reticulolithus*. In sample 6KA, the group of *Assipetra* + *Reticulolithus* is common, and *Nannoconus* spp. are frequent. In sample 25KA, common taxa are the group of *Assipetra* + *Reticulolithus* whereas *Nannoconus* spp. became very rare. Amongst very rare species, *Retecapsa angustiforata*, *Conusphaera mexicana mexicana* and *Micranolithus hoschulzii* are found in samples 1KA and/or 4KA, 6KA, and 25KA. One specimen of

*steinmannii* Kamptner, 1931; sample 1KA. **15, 16.** *Nannoconus globulus* subsp. *globulus* Bronnimann, 1955; sample 1KA. **17.** *Assipetra infracretacea* subsp. *larsonii* Tremolada et Erba, 2002; sample 1KA. **18.** *Assipetra infracretacea* (Thierstein, 1973) Roth, 1973; sample 25KA. **19.** *Reticulolithus terebrodentarius* subsp. *youngii* Tremolada et Erba, 2002; sample 1KA. **20.** *Reticulolithus terebrodentarius* Applegate et al. in Covington and Wise, 1987; sample 6KA. **21.** *Reticulolithus wisei* Thierstein, 1971; sample 1KA. **22, 23.** *Hayesites irregularis* (Thierstein in Roth and Thierstein, 1972) Applegate et al. in Covington and Wise, 1987; sample 1KA. **24.** *Lithraphidites carniolensis* Deflandre, 1963; sample 25KA. Scale bars: 5 µm (1–5, 7–21, 24), 2 µm (6, 22, 23).

Samples	Pyrite	Etching	Overgrowth	Abundance	<i>Assipetra infracretacea</i>	<i>Assipetra infracretacea larsonii</i>	<i>Conusphaera mexicana mexicana</i>	<i>Conusphaera rotthii</i>	<i>Cretarhabdus</i> sp.	<i>Crucililepisis cuvilli</i>	<i>Cyclagelosphaera margerellii</i>	<i>Diazomotolithus lehmani</i>	<i>Hayesites</i> sp.	<i>Hayesites irregularis</i>	<i>Helenea chlesia</i>	<i>Lithraphidites carniolensis</i>	<i>Micrancalithus hoschulzii</i>	<i>Micrancalithus obtusus</i>	<i>Nannoconus cornuta</i>	<i>Nannoconus globulus</i>	<i>Nannoconus kampfneri</i>	<i>Nannoconus steinmannii minor</i>	<i>Nannoconus steinmannii steinmannii</i>	<i>Nannoconus</i> sp.	<i>Relecapsa angustiflora</i>	<i>Rhagodiscus asper</i>	<i>Rotapilius laffitei</i>	<i>Rucinolithus terebrodentarius</i>	<i>Rucinolithus terebrodentarius youngii</i>	<i>Stauroolithites crux</i>	<i>Stauroolithites siasseri</i>	<i>Watznaueria barnesiae</i>	<i>Watznaueria biporta</i>	<i>Watznaueria britannica</i>	<i>Watznaueria communis</i>	<i>Watznaueria fossacincta</i>	<i>Watznaueria manivitiae</i>	<i>Zeugrhabdotus embigeri</i>	<i>Zeugrhabdotus scutula</i>
1KA	F	E3	O2	F	F	R	VR	VR	R	F	C	C	VR	C	F	VR	VR	R	R	F	R	R	VR	VR	VR	D	VR	VR	F	R	R	R							
2KA																																							
3KA																																							
4KA	R	E3	O2	R	F		VR		VR	F																													
5KA																																							
6KA	R	E3	O3	F	F		VR		VR	R	VR								R	R																			
7KA	R	E3	O3	T										VR																									
8KA		E3	O3	T																																			
9KA																																							
10KA	A			B																																			
11KA	A			B																																			
12KA	F			B																																			
13KA				B																																			
14KA				B																																			
15KA				B																																			
16KA	C			B																																			
17KA	C			B																																			
18KA	C			B																																			
19KA	C			B																																			
20KA				B																																			
21KA	C			B																																			
22KA	C			B																																			
23KA	C			B																																			
24KA	F			B																																			
25KA	C	E3	O3	R	A				VR	R		VR		VR	R																								
26KA	F			B																																			

**Fig. 8.** Distribution chart of calcareous nannofossils encountered in the Kalarytes section A. The nannofossil preservation was evaluated following the classes defined by Roth (1983). Class E3 and O3: samples with strongly etched and overgrown assemblages; Class E3-O2: samples with strongly etched and moderately overgrown assemblages. The abundance terminology per field of view (FOV) is from Lozar and Tremolada (2003). Codes for total abundance: F, few (11%–50% of all particles); R, rare (1%–10% of all particles); T, trace (< 1% of all particles); B, barren (no nannofossils are present). Codes for relative abundance of the recognized taxa: D, dominant (> 51% of the total assemblage); A, abundant (11%–50% of the total assemblage); C, common (1%–10% of the total assemblage); F, few (0.1%–1% of the total assemblage); R, rare (< 0.1% of the total assemblage); VR, very rare (< 1 specimen per 100 FOV). The same terminology is used for the relative abundance of pyrite.

*Hayesites* has been found in samples 1KA and 25 KA; it could be attributed to the species *H. irregularis* in sample 1KA. In sample 1KA, *Micrancalithus obtusus* and *Zeugrhabdotus scutula* have also been recognized.

### 5.1.2. Radiolarian

Surface features of many of the observed radiolarian tests are obscured by pyritization. The assemblages of samples 10KA, 11KA and 38KB are similar and dominated by the species *Holocryptocanium barbui* (Dumitrica, 1970). Seventeen radiolarian taxa have been recognized, including the age diagnostic species *Hiscocapsa asseni* (Tan, 1927), *Dictyomitria communis* (Squinabol, 1903), *Rhopalosyringium fossile* (Squinabol, 1903), and *Pseudodictyomitria lodogaensis* (Pessagno, 1977) (Figs. 9–11). Thin sections of rock samples from the stratigraphic level below the organic-rich horizon (e.g., sample 7KA; Fig. 12) showed the richness of radiolarian content in contrast to the absence of foraminifera.

### 5.2. Bulk organic geochemistry

The stratigraphic, isotopic and bulk organic matter characteristics of the 68 samples investigated are listed in Tables S1 and S2 (Appendix A) and illustrated in Fig. 13. The values of the total organic carbon content (TOC) are generally low (< 0.2 wt% of the bulk rock). Only two samples from section A (10KA and 11KA) and one sample from section B exhibit significantly higher concentration of organic matter (characteristic peaks in the curves of Fig. 13). The CaCO<sub>3</sub> content ranges between < 10 and 51.07 w/w for the samples of section A and between 0.94 and 89.95% for the samples

of section B. The determined *Tmax* values range from 341 to 470 °C for the samples of section A, and from 373 to 508 °C for the samples of section B.

### 5.3. Chemostratigraphy

#### 5.3.1. Pyrite clusters

The light microscope observation of the smear slides prepared from the samples of the section A and used for calcareous nannofossil semi-quantitative analyses showed the presence of pyrite clusters in almost all the stratigraphic levels of the section (Figs. 14, 15). They are particularly abundant in the black shale interval (samples 10KA and 11KA; Figs. 8, 14, 15).

#### 5.3.2. Stable carbon and oxygen isotopes

Carbon- and oxygen- isotope profiles through the studied sections are presented in Fig. 13. For the isotopic curve of the section A, despite the relative low sampling resolution throughout the investigated section, there is a sharp negative carbon isotope excursion concurrent with an abrupt increase in TOC values in the interval characterized by shale deposits. A synchronous negative δ<sup>18</sup>O excursion can also be observed. The relative high sampling resolution (every 5–10 cm) through section B allowed a more reliable separation and labeling of the different segments of the isotopic curve according to the reference C-isotope segments firstly described by Menegatti et al. (1998). Indeed, the bulk δ<sup>13</sup>C<sub>carb</sub>-values in limestone of the lower part of the Kalarytes section B exhibit features consistent with those observed in the pre-OAE 1a segment C2 of Menegatti et al. (1998) (Fig. 13). Just before the onset of the anoxic deposition, a clear negative shift in

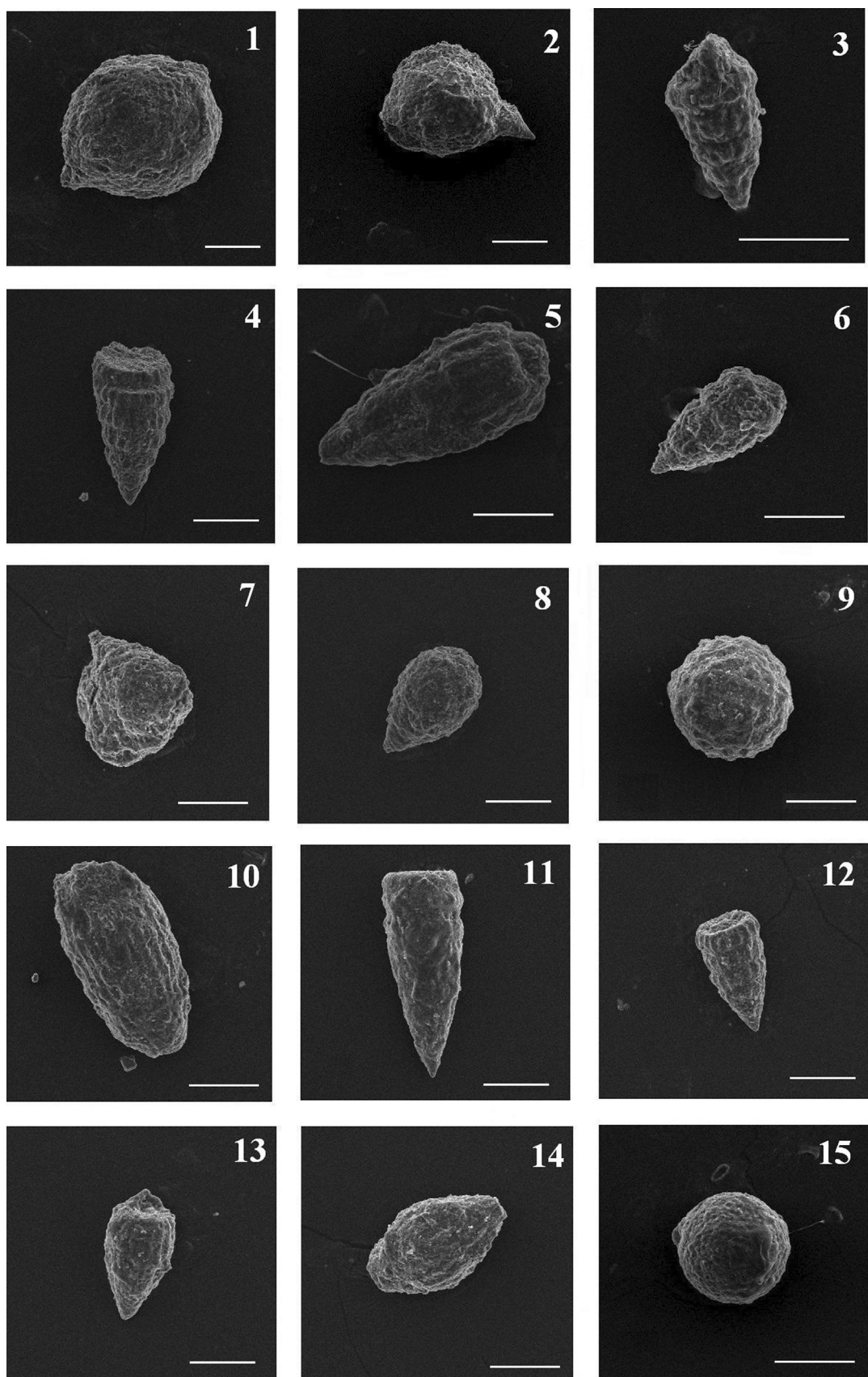


**Fig. 9.** SEM photomicrographs of radiolarians extracted from sample 10KA of the Kalarytes section A. **1.** *Sethocapsa orca* (Foreman, 1975). **2.** *Hiscocapsa asseni* (Tan, 1927). **3, 4.** **12.** *Dictyomitra communis* (Squinabol, 1903). **5.** *Pseudodictyomitra carpatica* (Lozyniak, 1969). **6.** *Xitus clava* (Parona). **7.** *Rhopalosyringium fossile* (Squinabol, 1903). **8.** *Sethocapsa uterculus* (Parona, 1890). **9.** *Praeconosphaera* sp. (Yang, 1993). **10.** *Archaeodictyomitra* sp. (Pessagno, 1976). **11.** *Pseudodictyomitra lodoxaensis* (Pessagno, 1977). **13.** *Thanarla brouweri* (Tan Sin Hok, 1927). **14.** *Archaeodictyomitra lacrimula* (Foreman, 1973). **15.** *Holocryptocanum barbui* (Dumitrica, 1970). Scale bars: 100 µm.

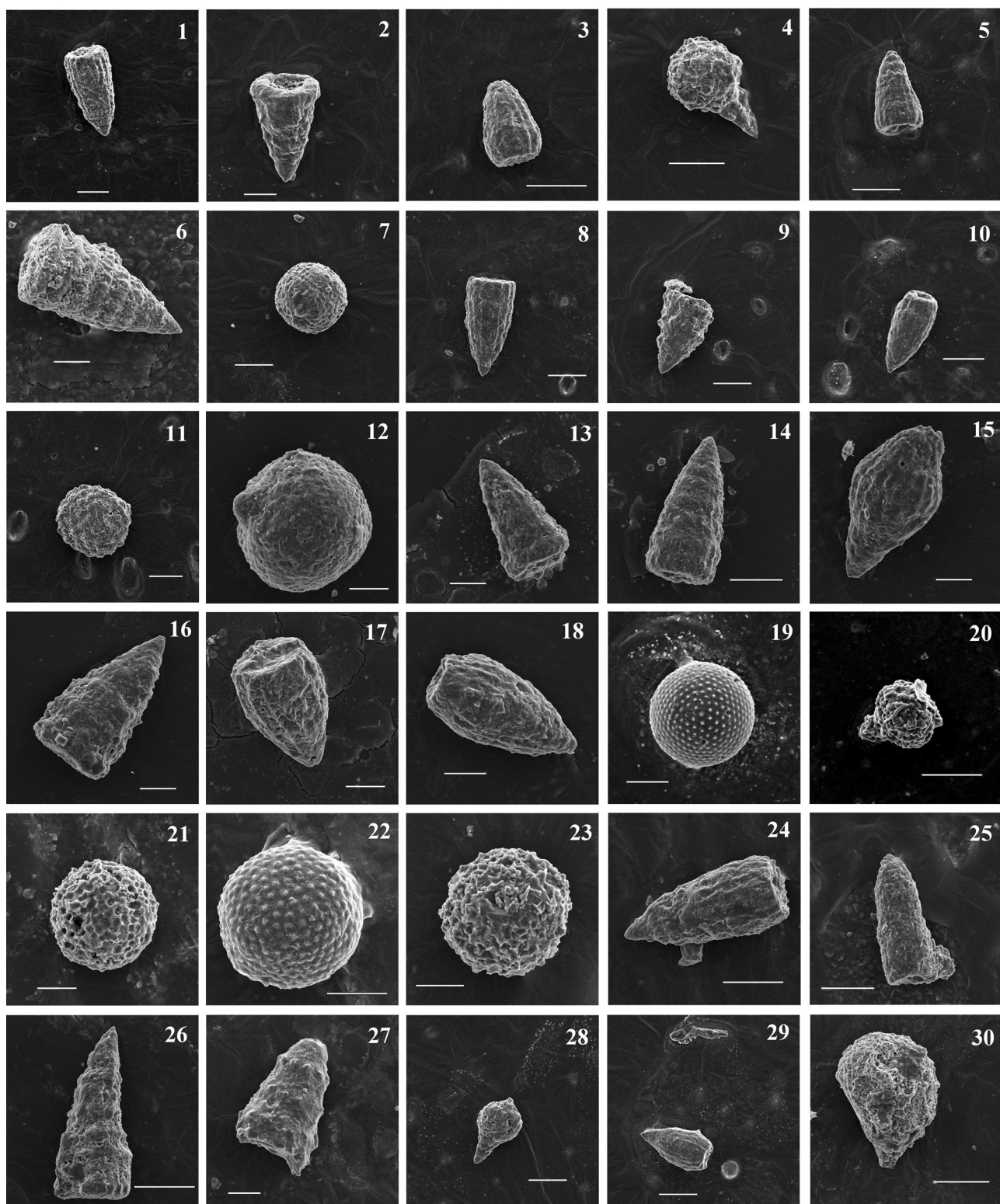


**Fig. 10.** SEM photomicrographs of radiolarians extracted from samples of Kalarytes B section. **1.** *Dictyomitra communis* (Squinabol, 1903); sample 8KB. **2.** *Xitus clava* (Parona); sample 8KB. **3.** *Thanarla brouweri* (Tan Sin Hok, 1927); sample 8KB. **4.** *Hiscocapsa asseni* (Tan, 1927); sample 8KB. **5.** *Dictyomitra communis* (Squinabol, 1903); sample 8KB. **6.** *Dictyomitra communis* (Squinabol, 1903); sample 36KB. **7.** *Holocryptocanium barbui* (Dumitrica, 1970); sample 8KB. **8.** *Dictyomitra communis* (Squinabol, 1903); sample 8KB. **9.** *Xitus clava* (Parona); sample 8KB. **10.** *Thanarla* sp. (Pessagno); sample 8KB. **11.** *Praeconosphaera* sp. (Yang, 1993); sample 8KB. **12.** *Sethocapsa orca* (Foreman, 1975); sample 11KB. **13.** *Xitus clava* (Parona); sample 11KB. **14.** *Pseudodictyomitra carpathica* (Lozyniak, 1969); sample 11KB. **15.** *Archaeodictyomitra lacrimula* (Foreman, 1973); sample 11KB. **16.** *Pseudodictyomitra carpathica* (Lozyniak, 1969); sample 11KB. **17.** *Thanarla brouweri* (Tan Sin Hok, 1927); sample 11KB. **18.** *Thanarla* sp. (Pessagno); sample 11KB. **19.** *Holocryptocanium barbui* (Dumitrica, 1970); sample 18KB. **20.** *Thanarla pacifica* Nakaseko et Nishimura; sample 18KB. **21.** *Praeconosphaera* sp. (Yang, 1993); sample 18KB. **22.** *Holocryptocanium barbui* (Dumitrica, 1970); sample 18KB. **23.** *Praeconosphaera* sp. (Yang, 1993); sample 18KB. **24.** *Pseudodictyomitra carpathica* (Lozyniak, 1969); sample 21KB. **25.** *Lithomitra* (*Archaeodictyomitra*) *excellens* (Tan Sin Hok 1927); sample 21KB. **26.** *Pseudodictyomitra carpathica* (Lozyniak, 1969); sample 21KB. **27.** *Xitus clava* (Parona); sample 32KB. **28.** *Hiscocapsa uterculus* (Parona); sample 8KB. **29.** *Thanarla brouweri* (Tan Sin Hok, 1927); sample 8KB. **30.** *Rhopalosyringium fossile* (Squinabol, 1903); sample 41KB. Scale bars: 100 µm (1, 3–5, 7–11, 14, 20, 24–26, 28–30), 50 µm (2, 6, 12, 13, 15–19, 21–23, 27).

Radiolarian species	Geological age					
	BERRIASIAN	VALANGINIAN	HAUTERIVIAN	BARREMIAN	APTIAN EARLY / LATE	ALBIAN
<i>Sethocapsa orca</i>						
<i>Hiscocapsa asseni</i>						
<i>Dictyomitra communis</i>						
<i>Pseudodictyomitria carpathica</i>						
<i>Xitus clava</i>						
<i>Rhopalosyringium fossile</i>						
<i>Sethocapsa uterculus</i>						
<i>Pseudodictyomitria lodogaensis</i>						
<i>Thanarla brouweri</i>						
<i>Archaeodictyomitra lacrimula</i>						

**Fig. 11.** Stratigraphic ranges of radiolarian species found in samples of the Kalarytes sections A and B.

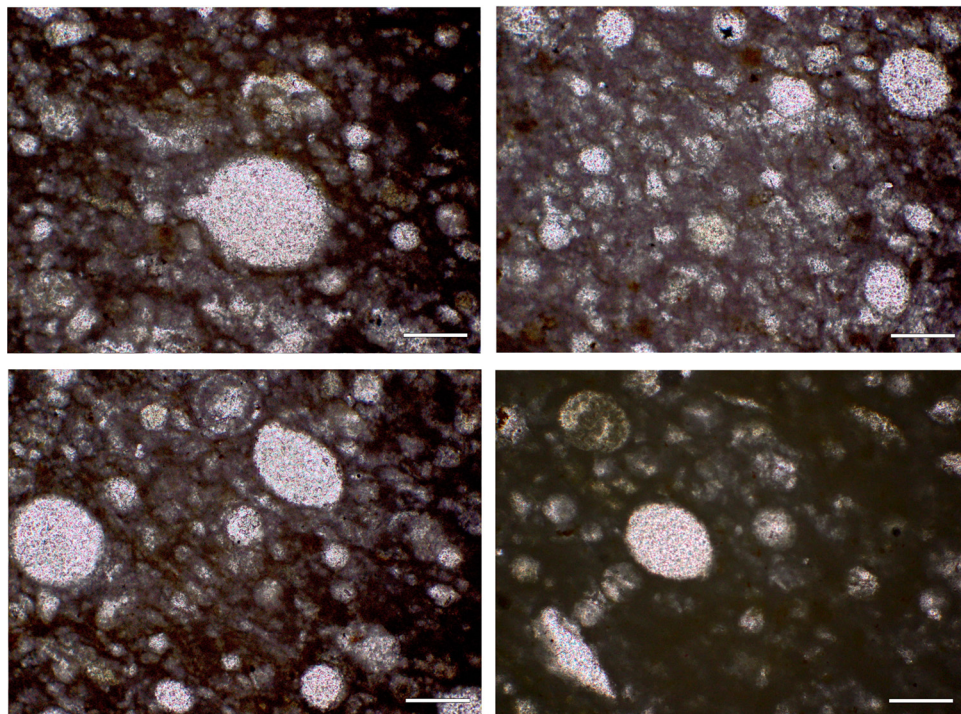


**Fig. 12.** Limestone containing numerous radiolarian in a micritic matrix. Thin section of sample 7KA (depth 7.23 m) under plane polarized light. Scale bars: 200  $\mu$ m.

$\delta^{13}\text{C}_{\text{carb}}$ -values (from 1.31 to  $-0.73\text{\textperthousand}$ ) is observed, reliably correlated with the sharp negative shift in  $\delta^{13}\text{C}_{\text{carb}}$  (segment C3 of Menegatti et al., 1998) that characterizes the basal part of the OAE 1a level in the Cismon section. Then  $\delta^{13}\text{C}_{\text{carb}}$  increases (segments C4–C5 of Menegatti et al. 1998). After a sharp decrease of  $\delta^{13}\text{C}_{\text{carb}}$  at the end of C5 (sample 7KA; Table S1, Appendix A), a return to background isotopic values (C6 and C7 segments) is observed in the isotopic curve of section A (Fig. 13).

### 5.3.3. Biomarker analysis

Representative GC-MS signals of the aliphatic fraction, total ion chromatogram (TIC) and  $m/z$  57 and  $m/z$  191 ion chromatograms are shown in Figs. 16–18. Based on these chromatograms, a series of biomarker compounds were identified and characteristic

geochemical indices were calculated using their peak areas (Table S4, Appendix A).

*n*-Alkanes are abundant in the aliphatic fraction of all analyzed extracts, with C-chain length ranging from  $C_{11}$  to  $C_{38}$  (Fig. 16). The average chain length (ACL) of *n*-alkanes, calculated after Cranwell (1973), ranges from 27.55 to 28.98 for the seven samples of the Kalarytes section A. The sample from section B has a relatively low ACL value (27.76; Table S4). The Carbon Preference Index (CPI) values of the seven analyzed samples of section A, calculated after Bray and Evans (1961), vary between 0.93 and 1.17 (Table S4), whilst the two highest values correspond to the organic-rich samples 10KA and 11KA. The sample 38KB from section B has an even higher value (1.56; Table S4). The studied samples from section A show OEP values (odd-even predominance; Scalan and

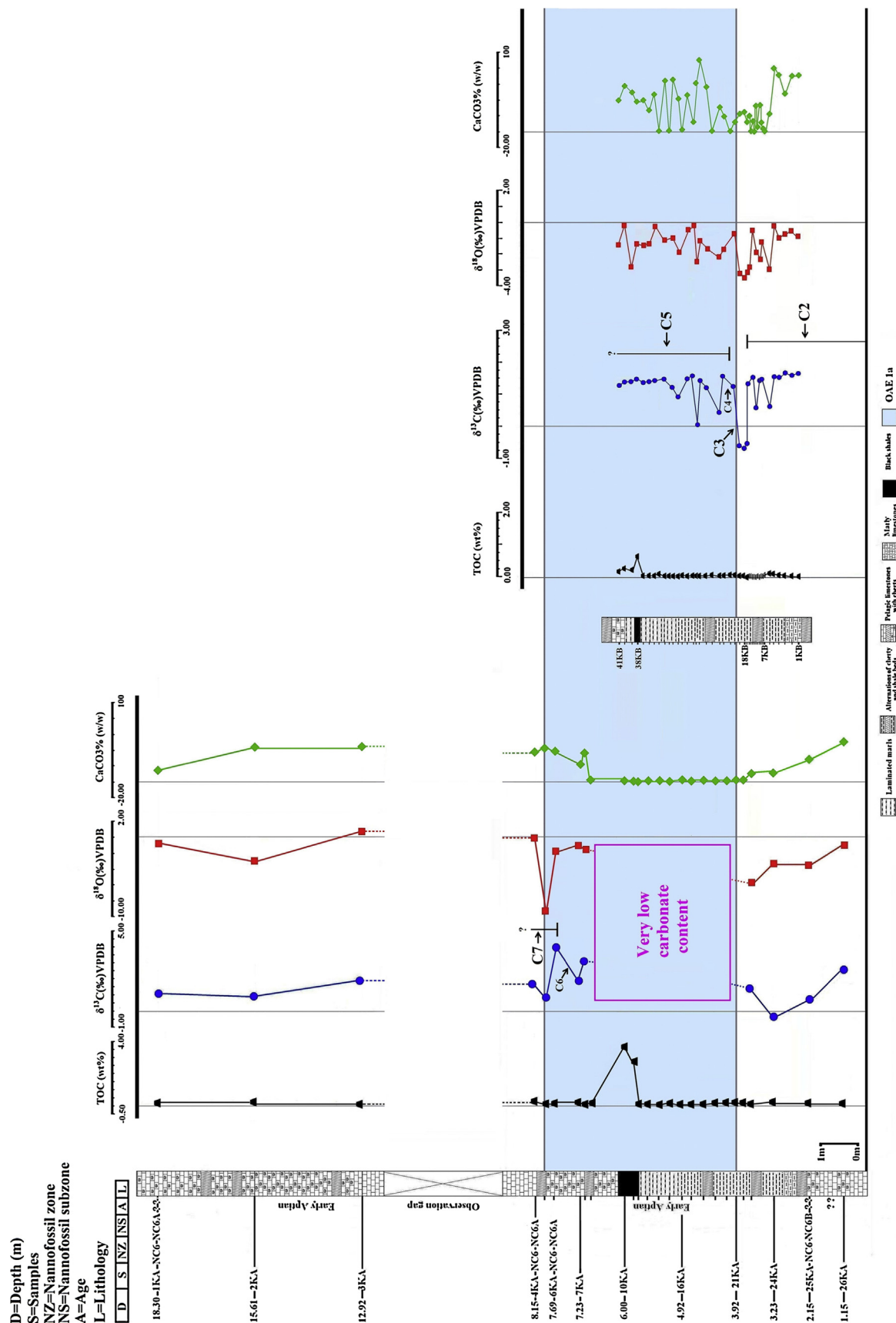


**Fig. 13.** Lithostratigraphic log, bulk geochemical and stable (C, O) isotope profiles through the Kalarytes sections A and B. Summary of biostratigraphic data based on observed distribution of calcareous nannofossils through the Kalarytes section A. Labels C2–C7 indicate segments of the stable isotope curves of the Kalarytes sections A and B corresponding to segments of reference stable isotope curves studied by Menegatti et al. (1998) in the pelagic carbonate sections of the Southern Alps of northern Italy (Cismon section) and Swiss Prealps (Roter Sattel section). The pale blue band indicates the chemostratigraphically defined OAE 1a.

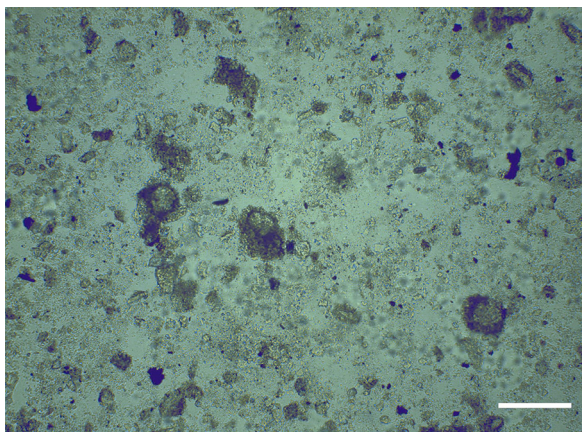


**Fig. 14.** Isolated and clustered pyrite framboids in association with microfossil fragments (possibly diatoms). Sample 7KA, depth 7.23 m. Smear slide photomicrograph under plane polarized light,  $\times 100$ . Scale bar: 200  $\mu\text{m}$ .

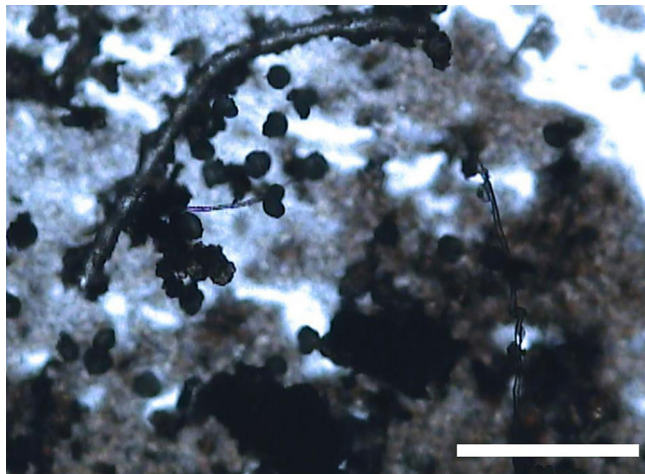


**Fig. 15.** Clusters of frambooidal pyrite associated with plant debris. Sample 10KA, depth 6.00 m. Smear slide photomicrograph under plane polarized light,  $\times 200$ . Scale bar: 100  $\mu\text{m}$ .

Smith, 1970) between 0.99 and 1.14. The sample 38KB from section B has a higher OEP value (1.54; Table S4).

In the samples the isoprenoids pristane and phytane were recognized; the pristane/phytane (Pr/Ph) ratio ranges between 0.14 and 1.60 for the samples of section A, and equals 0.35 for the only sample analysed from section B (Table S4). The  $R_{22}$  index (ten Haven et al., 1988) ranges from 0.85 to 2.43 for the samples of section A, and is 0.69 for the sample 38KB from section B. Lycopane was identified in the two organic-rich samples of the section A (10KA and 11KA), with lycopane/ $n$ -C<sub>31</sub> ratio of 0.65 and 0.28, respectively (Tables S4, S5; Appendix A). In the three organic-rich samples from both sections (10KA, 11KA, 38KB), biomarker compounds such as steranes, hopanes and terpanes were recognized. Among others, dinosterane was identified based on the spectrum published by Summons et al. (1987) (Figs. 17, 18).

In the aromatic fraction, various aromatic steroids were identified (Figs. 17, 18; Table S6, Appendix A).

In the aliphatic fraction of the samples 10KA, 11KA and 38KB (ion chromatogram  $m/z$  191), hopanoid compounds were recognized and considered for the calculation of the Ts/Ts+Tm ratio (0.41 and 0.23 for samples 11KA and 38KB, respectively), C<sub>30</sub> moretane/C<sub>30</sub> hopane ratio (0.27, 0.22 and 0.15, respectively), and C<sub>32</sub> 22S/22S+22R homohopane ratio (0.24, 0.41 and 0.46, respectively; Table S4, Appendix A). Gammacerane was recognized

only in samples 11KA and 38KB, giving gammacerane/C<sub>30</sub> hopane ratio values of 0.30 and 0.24, respectively (Table S4). Among the hopanoid compounds shown in the  $m/z$  191 ion chromatogram of sample 11KA are two methyl-hopanes (Fig. 17; Table S5, Appendix A). Their identification was based on the presence of the characteristic  $m/z$  205 fragment ion in their mass spectra, originating from a methyl group bound to the A-ring of the hopanes (Aguiar et al., 2011). The 2-Me-hopane index (cyanobacterial index) was calculated after Summons et al. (1999) for only one of the two organic-rich samples of section A in which were recognized a C<sub>32</sub>, 2-methyl-17 $\beta$ (H), 21 $\alpha$ (H)-homomoretane and a C<sub>32</sub>, 2-methyl-17 $\beta$ (H), 21 $\beta$ (H)-homohopane, coeluting with C<sub>31</sub>, 17 $\beta$ , 21 $\beta$ (H)-homohopane. The resulting cyanobacterial index value is 8.97%. Among the terpenoid compounds recognized in the samples are tricyclic terpanes (aliphatic fraction), phenanthrene, cadalene and retene, (aromatic fraction; Figs. 17, 18; Table S6, Appendix A). The retene/phenanthrene ratio was calculated for the two organic-rich samples of section A, with values of 0.07 and 0.31. The compound retene was not identified in the aromatic fraction of the sample 38KB.

## 6. Discussion

### 6.1. Chronostratigraphic framework

According to Tremolada and Erba (2002), the stratigraphic range of large-sized specimens of *Assipetra* (*A. infracretacea larsonii*) and *Rucinolithus* (*R. terebrodentarius youngii*) is Aptian. The recognition of the Barremian/Aptian boundary is linked to the first occurrence (FO) of *H. irregularis* (Thierstein, 1973; Bralower, 1987; Coccioni et al., 1992; Bralower et al., 1993), which is widely used as a basal Aptian marker at low latitudes (Bergen, 1994), whereas it is rare and sporadic in boreal sections (Bown et al., 1998). Cecca et al. (1994) have shown in two tethyan sections that the first appearance datum (FAD) of *H. irregularis* occurs in the uppermost part of the Tethyan *M. sarasini* ammonite zone and consequently predates the Barremian/Aptian boundary. Erba (2004) shows in a synthesis of major biotic events in the late Barremian–Aptian interval that a nannoconid decline occurs just before the FO of *H. irregularis*, which is followed by the first co-occurrences of both *A. infracretacea larsonii* and *R. terebrodentarius youngii*. Four species amongst taxa recognized in this study have their last occurrence (LO) in the early Aptian: first *C. rothii*/*C. mexicana*, then *N. steinmannii* and *R. angustiforata* (Bralower et al., 1993). Herrle and Mutterlose (2003) have shown that the late early Aptian interval is characterized by high abundances of large specimens of *Assipetra infracretacea* and *Rucinolithus terebrodentarius*. In the sample 1KA, overgrown specimens of *Crucilliepsis cuvilli* were observed, suggesting a reworking of older strata, since the normal extinction level of this species is late Hauterivian. Many publications mentioned the occurrence of this species in Barremian and early Aptian samples (Bralower et al., 1993; Erba et al., 1999; Channell et al., 2000; Lozar and Tremolada, 2003; Godet et al., 2010).

According to their general composition and more specifically because of the presence of specimens attributable to *H. irregularis* in the first studied sample 1KA, the assemblages recognized in the samples 1KA, 4KA, and 6KA can possibly be attributed to the Subzone NC6A, or *Conusphaera rothii* Subzone of Bralower et al. (1993), which corresponds to the interval from the FO of *H. irregularis* to the LO of *C. rothii*. The assemblages of the sample 25KA (collected from the interval with shales) characterized by common *Assipetra* and *Rucinolithus*, very rare *Nannoconus* spp., and the absence of *Conusphaera*, could be attributed to the Subzone NC6B, or *Grantarhabdus coronadventis* Subzone of Bralower et al. (1993), which corresponds to the interval from the LO of *C. rothii* to

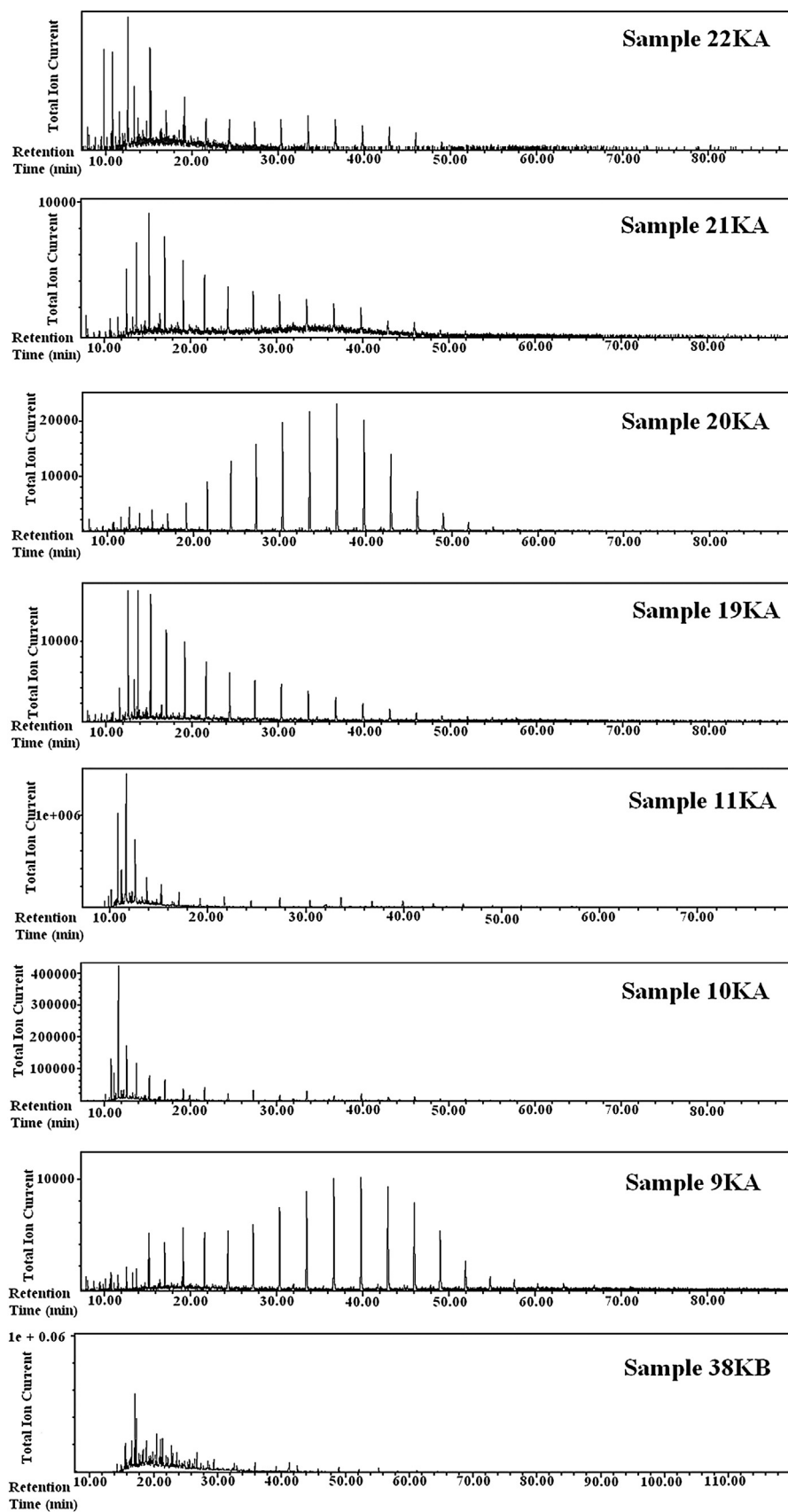


**Fig. 16.**  $m/z$  57 ion chromatograms of the aliphatic fraction of the analyzed samples showing the distribution of  $n$ -alkanes.

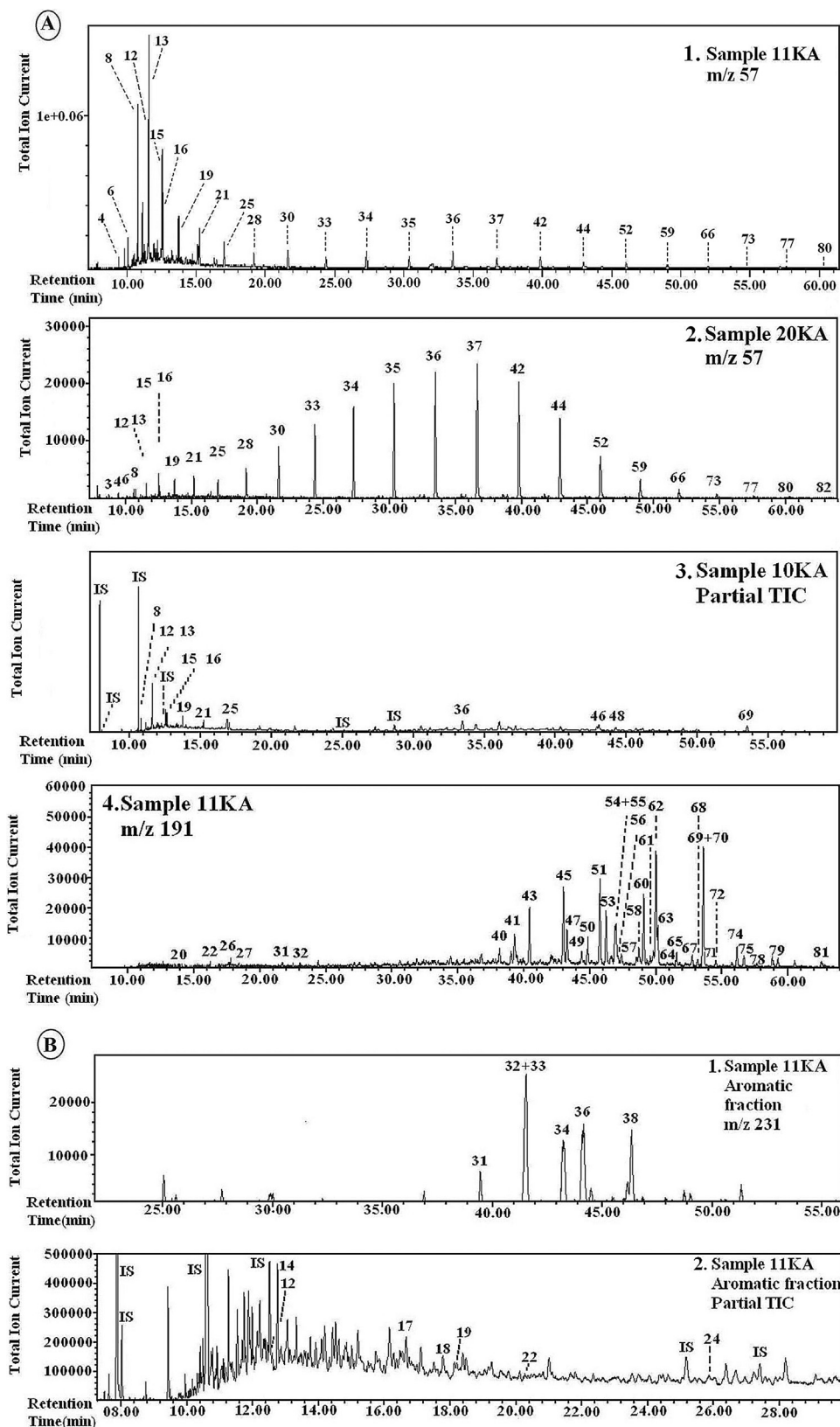


**Fig. 17.** A. Chromatograms of the aliphatic fraction of selected samples from the Kalarytes section A: 1:  $m/z$  57 ion chromatogram, sample 11KA; 2:  $m/z$  57 ion chromatogram, sample 20KA; 3: Partial Total Ion Current chromatogram, sample 10KA; 4:  $m/z$  191 ion chromatogram, sample 11KA. Peak assignments are given in Table S5 (Appendix A). B. Chromatograms of the aromatic fraction of selected samples from the Kalarytes Section A: 1:  $m/z$  231 ion chromatogram, sample 11KA; 2: Partial Total Ion Current chromatogram, sample 11KA. Peak assignments are given in Table S6 (Appendix A).

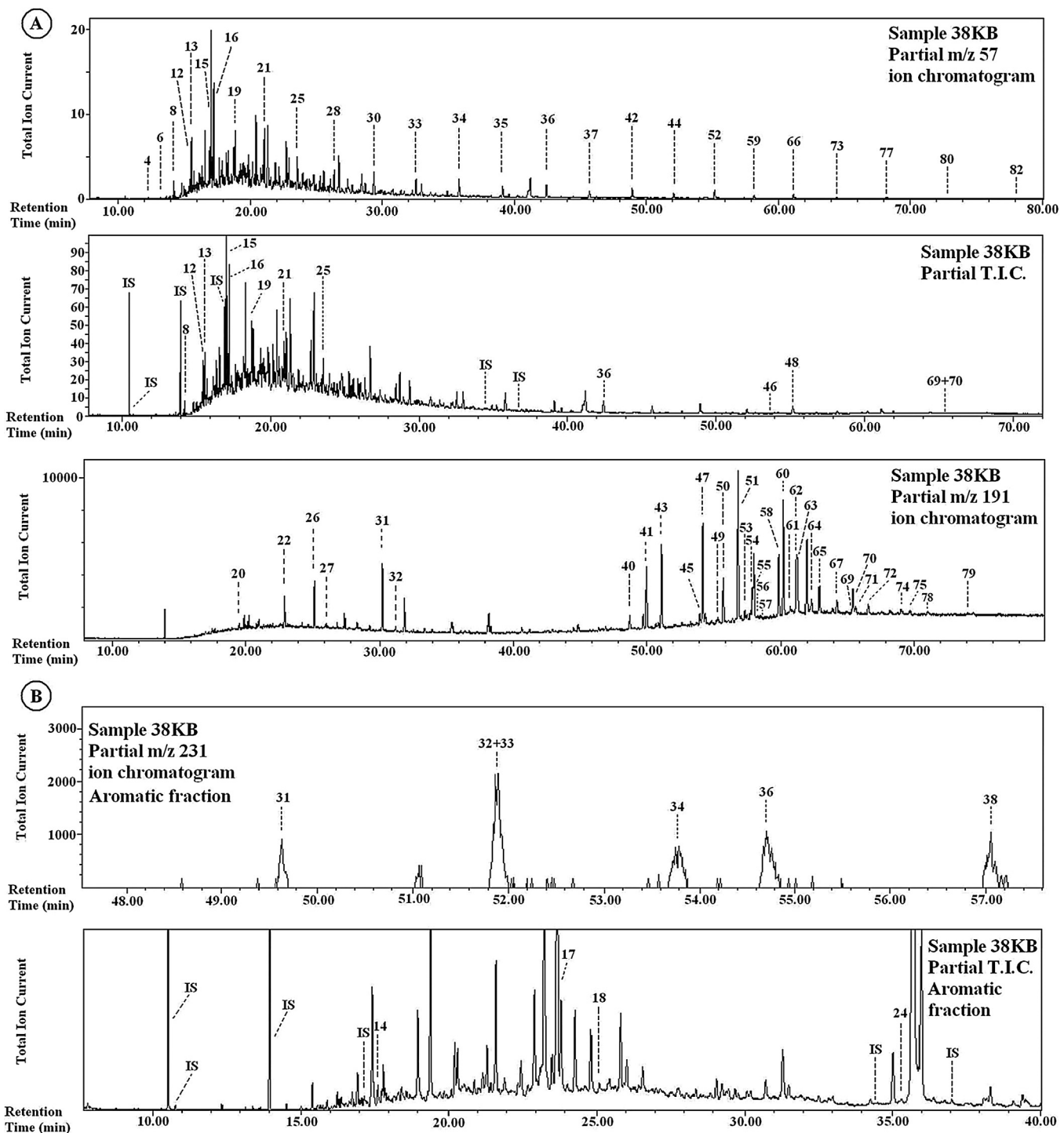


**Fig. 18.** A. Chromatograms of the aliphatic fraction of sample 38KB from the Kalarytes section B. top: Partial  $m/z$  57 ion chromatogram; middle: Partial Total Ion Current chromatogram; bottom: Partial  $m/z$  191 ion chromatogram. Peak assignments are given in Table S5 (Appendix A). B. Chromatograms of the aromatic fraction of sample 38KB from the Kalarytes section. Top: Partial  $m/z$  231 ion chromatogram; bottom: Partial Total Ion Current chromatogram. Peak assignments are given in Table S6 (Appendix A).

the FO of *Eprolithus floralis*. No specimens of *E. floralis* have been observed in the Kalarytes section A. All these data give an age of early to middle early Aptian for the four nannofossil-bearing samples of the Kalarytes section A (1KA, 4KA, 6KA and 25 KA; Figs. 7, 8, 13).

The scarcity of *Nannoconus* spp. recognized in the sample 25KA could correspond to the nannoconid crisis (Erba, 1994). It starts just before the OAE 1a and spans the entire event (Erba, 2004). The biostratigraphic evaluation of radiolarian assemblages was based on the biozonation scheme of Baumgartner et al. (1995). The

presence of key radiolarian taxa in the studied samples (Figs. 9–11) indicates an early Aptian age for the organic-rich horizons of the Kalarytes sections A and B, compatible with the age yielded from calcareous nannofossil data. It is worth noting here that the previous local biostratigraphic studies on the Pindos Zone did not date the Aptian–Albian interval directly, due to the absence or poor preservation of characteristic foraminifera (Fig. 12). This age was deduced by stratigraphic framing (Fleury, 1980; Degnan and Robertson, 1998; Neumann and Zacher, 2004). The early Aptian black shale intervals of the Kalarytes sections represent the local

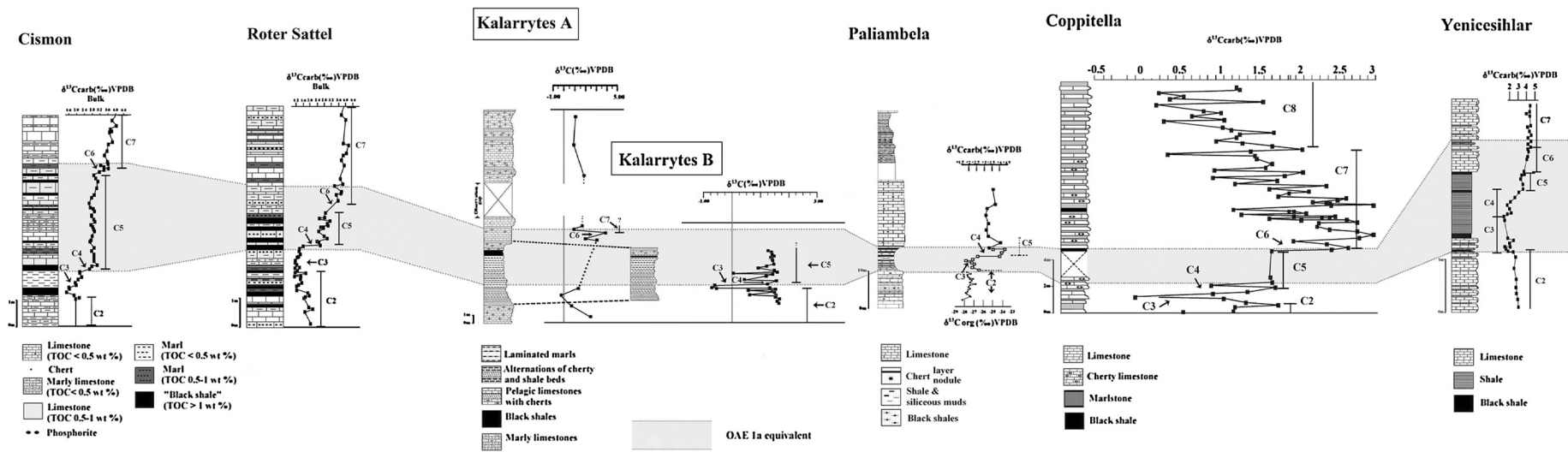


**Fig. 19.** Correlation of lithostratigraphic and stable carbon isotopic data from the Kalarytes sections A and B (this study; Pindos Zone, NW Greece) with those of the Cismon section (Menegatti et al., 1998; former eastern margin of the Alpine Tethys Ocean, southern Alps, northern Italy), Roter Sattel section (Menegatti et al., 1998; former western margin of the Alpine Tethys Ocean, Préalpes Médianes Romandes, western Switzerland), Paliambela section (Danellian et al., 2004; Ionian Zone, NW Greece), Coppitella section (Luciani et al., 2006; Apulia Platform, Southern Italy), and Yenicesihlar section (Hu et al., 2012; Sakarya Zone, Central Turkey). The stippled interval represents the OAE 1a (Sellia Event) equivalent, recorded in the studied sections.

lithological expression of the OAE 1a (Sell Event), as attested by the similarities between the isotopic curves, representing the bulk  $\delta^{13}\text{C}$  record of the sections A and B, and the comparable isotopic curves for the OAE 1a described by Menegatti et al. (1998) (Figs. 13, 19).

## 6.2. Paleoenvironmental interpretations of chemostratigraphic data

### 6.2.1. Euxinic depositional environments during the OAE 1a

It is known that the early Aptian OAE 1a represents an episode of global perturbation in the marine inorganic and the marine/terrestrial organic carbon reservoirs, due to excess burial of organic matter. The presence of pyrite in almost all stratigraphic levels of the Kalarytes section A, especially in the black shales interval where it is abundant, is an indication of the prevalence of sulphidic conditions (i.e., anoxic conditions in combination with high concentrations of hydrogen sulphide) during sedimentation (van Dongen et al., 2007). This is in accordance with other studies that document the presence of pyrite in sediments deposited during the OAE 1a in different locations. Bellanca et al. (2002) identified the Livello Selli equivalent in the biostratigraphically-constrained Aptian succession outcropping at Calabianca (NW Sicily). According to these authors on the basis of optical microscopy and SEM observations, pyrite occurs as small framboids ( $< 8 \mu\text{m}$ ), with major frambooidal pyrite in the lower part of the Livello Selli equivalent. Lechner et al. (2014) presented isotopic data obtained from lower Aptian shallow-water platform carbonates of the central Tethyan region. In the studied sections,  $\delta^{34}\text{S}$  shows a positive shift, coeval with the carbon-isotope positive excursion associated with the OAE 1a. This positive excursion is interpreted to reflect enhanced pyrite burial in marine sediments under euxinic conditions. These results imply that during OAE 1a oxygen-deficient waters spread over large areas, locally attaining euxinic conditions.

Regardless of their origin from oxic, dysoxic or euxinic environments, the majority of pyrite occurs in sedimentary rocks as spherical or irregularly shaped, single and clustered framboids, and rarely as euhedral crystals and replacements of organic matter (Wilkin et al., 1996). In euxinic environments, pyrite can form in the water column and settles to the sediment–water interface prior to burial (syngenetic pyrite), as well as *in situ* within the pore-waters of anoxic marine sediments underlying oxic water columns below the sediment–water interface (diagenetic pyrite; Raiswell and Berner, 1985). The pyrite formation in euxinic sediments is iron-limited and occurs before and after burial due to the lack of bioturbation. The DOP (Degree of Pyritization of Iron) values for oxic sediments are considerably lower than for euxinic and dysoxic sediments. These conditions result in higher concentrations of pyrite in euxinic sediments compared to oxic and dysoxic ones (Raiswell and Berner, 1985). This is compatible with the peak of pyrite framboids abundance recorded in samples 10KA and 11KA (Fig. 8).

According to Wilkin et al. (1996), pyrite framboids contained in modern sediments underlying sulphidic water columns are on average smaller and less variable in size than framboids from sediments underlying oxic or dysoxic water columns. The framboid size distribution is a property that does not significantly change during early diagenesis and can persist over geologic time. In the samples collected from the Kalarytes section A, rough pyrite framboids size distribution estimates were made under the light microscope. The abundant pyrite framboids in samples 10KA and 11KA are single, discrete, small (diameter  $< 20 \mu\text{m}$ ), spheroid and uniformly sized, whereas in the other samples of the section they are much fewer, slightly larger, irregularly shaped and in variable diameters (Figs. 14, 15).

The hydrogen sulphide needed for the formation of iron sulphides in anoxic environments is produced via bacterial reduction of sulphate by anaerobic microorganisms (van Dongen

et al., 2007). Hydrogen sulphide can also be produced during anaerobic oxidation of methane (Goldhaber, 2003; Burdige, 2006) performed by consortia of methanotrophic archaea and sulphate reducing bacteria (Hinrichs et al., 2000). The depth of the horizon where this reaction occurs, the sulphate/methane transition zone, depends on many factors (van Dongen et al., 2007).

### 6.2.2. Biotic responses, microbial community structure and primary productivity variations during the OAE 1a

The presence of iron sulphide nodules is in accordance with the presence of bacterial biomarkers in the studied samples (e.g., hopanoids), and also with biomarkers indicative of anoxic conditions in the depositional environment such as lycopane (Sinninghe Damsté et al., 2003) and gammacerane (Forster et al., 2004; Table S5, Appendix A). Possible sources of lycopane in marine environments are methanogenic archaea (e.g., Brassell et al., 1981) or photoautotrophic algae (e.g., Wakeham et al., 1993). Comet et al. (1981) reported a high abundance of lycopane, compared to *n*-alkanes, in samples from sediments deposited in an oxygen-depleted water-column setting, with surface waters characterized by high algal productivity. According to Sinninghe Damsté et al. (2003), the abundance of lycopane (usually coeluting with *n*-C35 alkane) has an implication for the past changes in the state of water-column oxygenation. The elevated values of the lycopane/*n*-C31 alkane ratio recorded empirically in sediments deposited under anoxic conditions have possibly originated from the greater vulnerability of the lycopane precursor compound to degradation under oxic conditions compared to *n*-alkanes. Lycopane was used from many authors as paleoredox indicator in various depositional settings (e.g., van Bentum et al., 2012), although its source organism is still unknown and the interpretation of the lycopane/*n*-C31 ratio values is difficult due to the multistep natural biogeochemical processes of land-derived, long-chain *n*-alkanes degradation and lycopane production (Sinninghe Damsté et al., 2003).

Gammacerane is a C30 pentacyclic triterpenoid, derived presumably from tetrahymanol, a compound with various possible source organisms (ciliates, ferns, fungi, bacteria). The occurrence of abundant gammacerane in sediments deposited under evaporitic conditions lead many authors in the past to suggest this as an indicator of hypersalinity. According to ten Haven et al. (1985), the ratio gammacerane/C<sub>30</sub> 17 $\alpha$ (H), 21 $\beta$ (H) hopane increases in hypersaline environments. Now it is clear that gammacerane is not necessarily restricted to this type of deposits. Sinninghe Damsté et al. (1995) suggested a pathway for the biosynthesis of its precursor compound tetrahymanol in predatory ciliates living at or below the aerobic-anaerobic interface of a stratified water column and feeding exclusively on anaerobic prokaryotic organisms like green and purple sulphur bacteria, and sulphide oxidizing bacteria. Dominance of bacteria and absence of eukaryotic organisms are expected in anaerobic environments. Since these conditions are necessary for the formation of tetrahymanol, its diagenetic product – gammacerane – in sediments could be considered as an indicator for water column stratification, typical in various euxinic environments.

The isoprenoids pristane and phytane are primarily derived from the chlorophyll's phytol side chain (e.g., Didyck et al., 1978). However, alternative sources, such as archaeabacterial ether lipids for both molecules (Didyck et al., 1978), or tocopherols for pristane (Brassell et al., 1983), have been proposed, which could complicate paleoenvironmental reconstructions. The pristane/phytane ratio is often used as an indicator of redox conditions of the depositional environment (Forster et al., 2004). The values of Pr/Ph ratio calculated for the two organic-rich samples of the section A (10KA and 11KA: 1.36 and 1.60, respectively; Table S4, Appendix A) are not indicative of anoxic conditions. Nevertheless, it should be

mentioned that this ratio may be influenced by the thermal maturity level, as the abundance of both compounds in the free hydrocarbon fraction is affected by their thermal generation from precursors and their liberation from the bound biomarker fraction (Koopmans et al., 1999). Consequently, according to Volkman and Maxwell (1986) the pristane/phytane ratio should be used with caution for the assessment of paleoredox conditions. Indications for the thermal immaturity of the two organic-rich samples of the section A are derived independently from the C30 moretane ( $\beta\alpha$  hopane)/C30( $\beta\beta+\alpha\beta$ )hopane ratio values (Mackenzie et al., 1980; Seifert and Moldowan, 1980; Peters et al., 2005), the C32 22S/22S+22R homohopane ratio values (Ensminger, 1977), the Ts/Ts+Tm ratio value (Seifert and Moldowan, 1978; Moldowan et al., 1986), the CPI values (Bray and Evans, 1961), and the OEP values (Scalan and Smith, 1970; Table S4, Appendix A).

$T_{max}$  values of 421 and 422 °C for samples 10KA and 11KA, respectively (Table S1, Appendix A), are indicative of the thermal immaturity of the organic matter and support the hypothesis that the primary organic signal is not affected by thermal alteration. Conversely, there are geochemical evidences (Ts/Ts+Tm ratio, C30 moretane/C30 hopane ratio, C32 22S/22S+22R homohopane ratio, CPI and OEP values, and  $T_{max}$  value of 436 °C) for the thermal maturity of the organic-rich sample 38KB from section B. Following the above mentioned evidences, the pristane/phytane ratio calculated for this sample (0.35; Table S4, Appendix A) would be indicative for anoxic conditions.

From the interpretation of *n*-alkanes distribution (Eglinton and Hamilton, 1967; Tissot et al., 1977; Simoneit et al., 1991; Brocks and Summons, 2003) and the presence of various biomarkers (hopanes, irregular isoprenoids, terpenoids) in the analyzed samples from the Kalarrytes section A, arises an initial estimation that the organic matter in the black shales interval of this section is dominantly derived from marine algal, microbial, cyanobacterial, and possibly archaeal sources with varying contributions of terrestrial plant material. In the sample 38KB Kalarrytes section B) were also found abundant marine algal, microbial and cyanobacterial biomarkers, but not many evidences for an archaeal or terrestrial contribution.

Dinosterane was identified in the most organic-rich samples from both sections (Fig. 17); this compound belongs to the group of C30 steranes, the most diagnostic biomarkers for marine depositional environments (Peters et al., 1986). Steranes originate from sterols of eukaryotic organisms (Volkman and Maxwell, 1986). Dinoflagellates are the only organisms reported to date to biosynthesize predominantly 4-methyl sterols (precursor compounds of dinosterane). They are the only organisms to contain sterols with the dinosteroid skeleton in significant amounts (Thomas et al., 1993). In the present oceans, dinoflagellates, diatoms and coccolithophores are the most prominent members of phytoplanktonic communities (Thomas et al., 1993), and it is expected that there is a significant contribution from these organisms to recent marine sediments. Hypothetically, dinoflagellates were important contributors to the organic matter deposited during the OAE 1a. It should be mentioned that Volkman et al. (1989) reported the presence of dinosterol (precursor of dinosterane) in a marine diatom, thus the use of dinosterane as a specific dinoflagellates marker needs caution (Thomas et al., 1993). However, this compound seems to be restricted to marine environments (Summons and Capon, 1988). Dinoflagellates are organisms that are resistant to variations in salinity and other environmental conditions (Volkman et al., 1999). The finding of dinoflagellates cysts in rock samples where dinosterane was also identified could be interpreted as additional evidence of its origin from these organisms.

The dominance of prokaryotic organisms in the organic matter shown by the hopanoid abundance in samples 10KA, 11KA and

38KB (Table S5, Appendix A) may be related to the presence of large cyanobacterial populations as likely contributors of these compounds in the depositional paleoenvironment. More specifically, the occurrence of 2 $\beta$ -methylhopanes in the aliphatic fraction of sample 11KA (Fig. 17; Table S5, Appendix A) indicates the presence of cyanobacteria in the corresponding interval (Dumitrescu and Brassell, 2005; van Breugel et al., 2007; Aguiar et al., 2011). The 2 $\alpha$ -methylhopanes have lost their biological configuration and are common in mature sediments and oils; they probably originate from the biogenic, relative unstable 2 $\beta$ -methylhopanes. According to Aguiar et al. (2011), 2 $\alpha$ -methylhopanes, originating from cyanobacteria, generally characterize marine samples whereas lacustrine ones are often enriched in 3 $\beta$ -methylhopanes.

Kuypers et al. (2004) suggested that cyanobacteria were the major primary producers during the OAE 1a in the Tethys Sea (Cismon, Italy) and Pacific Ocean (DSDP Site 463), as inferred from the observed abundance of the cyanobacterial lipid biomarkers (2-methylhopanoids). According to Kashiyama et al. (2008), during the OAE 1a in the western Tethys Sea, the nitrogen used by the photoautotrophic community was supplied mostly via N<sub>2</sub> fixation by cyanobacteria. Dumitrescu et al. (2006) also suggested a major contribution of cyanobacterial organic matter in the OAE 1a black shales from the Pacific Ocean (Shatsky Rise, ODP Leg 198), based on the abundance of 2-methylhopanoids. Ratios of methylhopanes to hopanes such as the cyanobacterial index are calculated as source indicators, thus reflecting the composition of bacterial populations during sedimentation (Aguiar et al., 2011). The determined value of cyanobacterial index in the present study is relatively low in comparison with the results reported by van Breugel et al. (2007) for Cismon, Italy, and DSDP Site 463, Mid-Pacific Mountains. In the Goguel level, southeastern France, the 2-MHI (cyanobacterial index) is between 5 and 25%, but its algae are produced as minor component after the OAE 1a (2-MHI < 5%; Ando et al., 2013). Furthermore, the already mentioned value does not provide strong evidence for a significant contribution of cyanobacteria to the sedimentary organic matter because it was calculated for only one representative sample from the Kalarrytes section A. A high-resolution, targeted biomarker study is needed to further decipher this situation.

There are many evidences that during OAE 1a and OAE 2, oceanic conditions favoring the prevalence of cyanobacteria among other phytoplanktonic groups were developed. This is a noticeable feature of Cretaceous OAEs (Asif and Fazeelat, 2012; Capone et al., 2005; Dutta et al., 2011; Lee and Brocks, 2011; Pedentchouk et al., 2004; Kuypers et al., 2004; Dumitrescu et al., 2006; Ando et al., 2013). A clear variation of the organic matter sources during the development of the studied anoxic event can be inferred from the biomarker analysis data of the Kalarrytes section A. A mixed origin of the organic matter during some intervals of this section (e.g., from the depth of 6.00 to 5.92 m) cannot be excluded. In these intervals, terrestrial organic matter coexists with organic matter from marine phytoplanktonic communities in different proportions, as biomarker data indicate (Tables S5, S6; Appendix A). For the black shale interval of the Kalarrytes section B, there are abundant biomarker evidences of a purely marine origin of the organic matter with negligible terrestrial contributions.

According to Okano et al. (2007) who analyzed rock samples from the Goguel level (OAE 1a), and Kilian and Paquier levels (OAE 1b) in the Vocontian Basin (southeastern France), there is no evidence for terrestrial input during the OAE 1a, in contrast to the OAE 1b. In samples 10KA and 11KA there are many evidences for terrigenous input in the organic-rich deposits. The variable presence of high molecular weight n-alkanes through the Kalarrytes section A could be an evidence of terrestrial organic matter, as can be seen in the chromatograms of

**Figs. 16 and 17.** Apart from the CPI values (Table S4, Appendix A) interpreted after Bray and Evans (1961), an additional evidence for significant terrigenous input arises from the presence of tricyclic terpanes in the aliphatic fraction of samples 10A and 11A (Greenwood and George, 1999; Greenwood et al., 2000), and terpenoid compounds such as cadalene and retene, a terrigenous biomarker with high specificity originated from gymnosperm plants (mostly conifers) in the aromatic fraction of these samples (Simoneit et al., 1993; Table S6, Appendix A). The aromatic fraction of sample 38KB is characterized by the absence of these compounds. In samples 10KA and 11KA, the values calculated for the retene/phenanthrene index are relative high. This evidence is compatible with the observations of Dumitrescu and Brassell (2005) and van Breugel et al. (2007). According to these authors, there is a significant contribution of terrestrial organic matter during OAE 1a, although this contribution has not been universally recorded in all studied sections as a typical situation for this anoxic event.

### 6.3. Correlations with coeval OAE 1a levels in the surrounding regions

The Kalarytes sections A and B, corresponding to an oceanic environment, are compared with the Paliambela section of NW Greece (Danelian et al., 2002, 2004). These paleogeographic areas are separated by the extensive Gavrovo-Tripolis carbonate platform. The Paliambela section belongs to the Ionian Basin, an epicontinental basin formed during the Pliensbachian (Early Jurassic) into the huge Apulia Platform and since then separated from the Pindos Ocean by the Gavrovo-Tripolis platform (Karakitsios, 1995). Consequently, the observed differences between the sections of these areas mainly relate to the thicker and more organic-rich alternating anoxic horizons in the Paliambela section (TOC content ranging from 0 to 6.65%). These differences reflect the restricted environment of the Ionian epicontinental sea, which locally enhanced anoxic conditions during OAE 1a, as documented by the presence of rich source rock horizons in many stratigraphic levels (Karakitsios, 1995, 2013). The reduced thickness of the Kalarytes anoxic horizons is due to the condensed sedimentation of the Pindos sequence, which is consistent with its oceanic nature. Nevertheless, all three sections present low calcium carbonate content within the OAE 1a horizon and a blooming of radiolarian populations as a result of enhanced paleoproductivity (Danelian et al., 2002). Samples from these sections exhibit similarities concerning the radiolarian composition (e.g., presence of *Dictyomitra communis* and *Pseudodictyomitra carpathica*). Additionally, the anoxic horizons of Kalarytes A and Paliambela sections are characterized by thermal immaturity (similar *Tmax* values), and they were also deposited under euxinic conditions as suggested by the presence of pyrite.

Graziano (2013) correlated the OAE 1a in the Apulia Carbonate Platform Margin-Ionian Basin system (Gargano Promontory, southeastern Italy) with pelagic sections of the Ionian basin (Coppitella, eastern Gargano, and Paliambela, northwestern Greece). He concluded that the Apulia shallow-water ecosystem reacted to the environmental disruptions leading to the onset of the OAE 1a sooner than that of the Coppitella and Paliambela sections, corresponding to more open sea environments. Consequently, this difference is more clearly expressed in the Kalarytes sections which represent an oceanic environment.

Hu et al. (2012) studied the OAE 1a along the pelagic Yenicesihlar section (Mudurnu, central Turkey). This oceanic depositional environment is equivalent to the one represented by the distant Kalarytes sections, as illustrated by the similarities concerning the lithology, the anoxic horizon thickness and the TOC values, ranging from 0.9 to 2.05%. Nevertheless, the slightly

different isotopic curves reflect the diversified local records of the OAE 1a. These correlations are presented in Fig. 19.

## 7. Conclusions

The present study is the first documentation of the OAE 1a in the Pindos oceanic sequence of Western Greece. The characteristic isotopic excursion of this anoxic event is well documented (particularly for the Kalarytes section B), constrained by calcareous nannofossil and radiolarian biostratigraphic data in the time interval of early to middle early Aptian. The prevalence of anoxic conditions during this time interval leading to the preservation of the sedimented organic matter is attested from the geochemical data (maximum TOC value 3.65%). The presence of pyrite in the black shale stratigraphic level of the Kalarytes section A is an important indication of the marine anoxia together with the high concentration of hydrogen sulphide. Biomarker analyses show mostly immature organic matter of predominantly marine origin with terrigenous contribution (lower in the case of the Kalarytes section B). Among the main source organisms of the organic matter are dinoflagellates, bacteria and cyanobacteria, as evidenced by the presence of dinosterane, hopanoids, and methyl-hopanoids, respectively. The characteristics of the Pindos organic-rich deposits show noticeable similarities with coeval early Aptian strata where the impact of OAE 1a has also been previously recorded.

## Acknowledgements

This work was funded by the National and Kapodistrian University of Athens project KAPODISTRIAS 70/4/11708. We thank Dr Elisabetta Erba, Dr José Manuel Castro, and two anonymous reviewers for their constructive comments on earlier versions of the manuscript. We thank Dr Marc de Rafelis for the isotopic analyses of the Kalarytes section B samples, Eleni Hamilaki for facilitating the sample preparation for GC-MS analysis, and Dr Elisabeth Stathopoulou for her assistance in SEM imaging of the samples.

## Appendix A. Supplementary data

Supplementary data (including Tables S1–S6) associated with this article can be found, in the online version, at <https://doi.org/10.1016/j.geobios.2018.04.006>.

## References

- Aguado, R., de Gea, G.A., Castro, J.M., O'Dogherty, L., Quijano, M.L., Naafs, D.B.A., Pancost, R.D., 2014. Late Barremian–early Aptian dark facies of the Subbetic (Betic Cordillera, southern Spain): Calcareous nannofossil quantitative analyses, chronostratigraphy and palaeoceanographic reconstructions. *Palaeogeography Palaeoclimatology Palaeoecology* 395, 198–221.
- Aguiar, A., Aguiar, H.G.M., Azevedo, D.A., Aquino Neto, F.R., 2011. Identification of methylhopane and methylmordanane series in Ceará Basin Oils Brazil, using comprehensive two-dimensional gas chromatography coupled to Time-of-Flight mass spectrometry. *Energy and Fuels* 25, 1060–1065.
- Ando, A., Kakegawa, T., Takashima, R., Saito, T., 2002. New perspective on Aptian carbon isotope stratigraphy: data from  $\delta^{13}\text{C}$  records of terrestrial organic matter. *Geology* 30, 227–230.
- Ando, A., Kaiho, K., Kawahata, H., Kakegawa, T., 2008. Timing and magnitude of early Aptian extreme warming: Unraveling primary  $\delta^{18}\text{O}$  variation in indurated pelagic carbonates at Deep Sea Drilling Project Site 463, central Pacific Ocean. *Palaeogeography Palaeoclimatology Palaeoecology* 260, 463–476.
- Ando, T., Sawada, K., Takashima, R., Nishi, H., 2013. Paleoproductivity of dinoflagellate and cyanobacteria during the mid-Cretaceous oceanic anoxic events in the Vocontian Basin SE France. *26th IUGS Organic Geochemistry: trends for the 21st Century* 2, 330–331.
- Argyriadis, I., De Graciansky, P.C., Marcoux, J., Ricou, L.E., 1980. The opening of the Mesozoic Tethys between Eurasia and Arabia-Africa. In: Aubouin, J., Debelmas, J., Latreille, M. (Eds.), *Géologie des chaînes alpines issues de la Téthys*, 26th International Geological Congress, Paris, Colloque C5. Bureau de Recherches Géologiques et Minières Mémoire, 115, pp. 199–214.

- Arthur, M.A., 2000. Volcanic contributions to the carbon and sulfur geochemical cycles and global change. In: Sigurdsson, H., Houghton, B., McNutt, S.R., Rymer, H., Stix, J. (Eds.), Encyclopedia of Volcanoes. Academic Press, San Diego, pp. 1045–1056.
- Asif, M., Fazeelat, T., 2012. Petroleum geochemistry of the Potwar Basin Pakistan: II – Oil classification based on heterocyclic and polycyclic aromatic hydrocarbons. *Applied Geochemistry* 27, 1655–1665.
- Aubouin, J., Bonneau, M., Davidson, G.J., Leboulenger, P., Matesko, S., Zambetakis, A., 1976. *Esquisse structurale de l'Arc égéen externe : des Dinarides aux Taurides*. Bulletin de la Société géologique de France 7 (18), 327–336.
- Baumgartner, P.O., Bartolini, A., Carter, E.S., Conti, M., Cortese, G., Danielian, T., De Wever, P., Dumitrica, P., Dumitrica-Jud, R., Gorican, S., Guex, J., Hull, D.M., Kito, N., Marcucci, M., Matsuoka, A., Murchev, B., O'Dogherty, L., Savary, J., Vishnevskaya, V., Widz, D., Yao, A., 1995. Middle Jurassic to Early Cretaceous radiolarian biochronology of Tethys based on Unitary Associations, middle Jurassic to Lower Cretaceous radiolaria of Tethys: occurrences, systematics, biochronology. In: Baumgartner, P.O., O'Dogherty, L., Gorican, S., Urquhart, E., Pillevuit, A., De Wever, P. (Eds.), Middle Jurassic to Lower Cretaceous Radiolaria of Tethys: Occurrences, Systematics, Biochronology, 23, Mem. Geol. (Lausanne), pp. 1013–1048.
- Bellanca, A., Erba, E., Neri, R., Premoli Silva, I., Sprovieri, M., Tremolada, F., Verga, D., 2002. Paleoceanographic significance of the Tethyan Livello Sellì (early Aptian) from the Hyblan Formation, northwestern Sicily: biostratigraphy and high-resolution chemostratigraphic records. *Palaeogeography Palaeoclimatology Palaeoecology* 185, 175–196.
- Bergen, J.A., 1994. Berriasian to early Aptian calcareous nannofossils from the Vocontian Trough (SE France) and Deep Sea Drilling Site 534: new nannofossil taxa and a summary of low-latitude biostratigraphic events. *Journal of Nannoplankton Research* 16, 59–69.
- Bernoulli, D., De Graciansky, P.C.D., Monod, O., 1974. The extension of the Lycian Nappes (SW Turkey) into the Southeastern Aegean Islands. *Eclogae Geologicae Helvetiae* 67, 39–90.
- Bonneau, M., 1982. Evolution géodynamique de l'Arc égéen depuis le Jurassique supérieur jusqu'au Miocène. *Bulletin de la Société géologique de France* 7 (24), 229–242.
- Bonneau, M., 1984. Correlation of the Hellenide nappes in the south-east Aegean and their tectonic reconstruction. In: Dixon, J.E., Robertson, A.H.F. (Eds.), The geological Evolution of the Eastern Mediterranean, 17, Geological Society of London, Special Publication, pp. 517–552.
- Bottini, C., Cohen, A.S., Erba, E., Jenkyns, H.C., Coe, A.L., 2012. Osmium-isotope evidence for volcanism, weathering, and ocean mixing during the early Aptian OAE 1a. *Geology* 40, 583–586.
- Bottini, C., Erba, E., Tiraboschi, D., Jenkyns, H.C., Schouten, S., Sinninghe Damsté, J.S., 2015. Climate variability and ocean fertility during the Aptian Stage. *Climate of the Past* 11, 383–402.
- Bown, P.R., Rutledge, D.C., Crux, J.A., Gallagher, L.T., 1998. Lower Cretaceous. In: Bown, P.R. (Ed.), *Calcareous Nannofossil Biostratigraphy*. British Micropalaeontological Society Series. Chapman and Hall/Kluwer Academic Publishers, London, pp. 86–131.
- Bralower, T.J., 1987. Valanginian to Aptian calcareous nannofossil stratigraphy and correlation with the upper M-sequence magnetic anomalies. *Marine Micropaleontology* 11, 293–310.
- Bralower, T.J., Sliter, W.V., Arthur, M.A., Leckie, R.M., Allard, D., Schlanger, S.O., 1993. Dysoxic/anoxic episodes in the Aptian-Albian (Early Cretaceous). In: Pringle, M.S., Sager, W.W., Sliter, W.V., Stein, S. (Eds.), *The Mesozoic Pacific: Geology, Tectonics, and Volcanism*, 77, American Geophysical Union, Geophysical Monograph, pp. 5–37.
- Bralower, T.J., Leckie, R.M., Sliter, W.V., et al., 1995. An integrated Cretaceous microfossil biostratigraphy. In: Berggren, W.A., Kent, D.V., Aubry, M.P. (Eds.), *Geochronology, time scales and global stratigraphic correlation*, 54, Society of Economic Paleontologists and Mineralogists, London, Special Publication, pp. 65–79.
- Brassell, S.C., Wardrop, A.M.K., Thomson, I.D., Maxwell, J.R., Eglinton, G., 1981. Specific acyclic isoprenoids as biological markers of methanogenic bacteria in marine sediments. *Nature* 290, 693–696.
- Brassell, S.C., Eglinton, G., Maxwell, J.R., 1983. The geochemistry of terpenoids and steroids. *Biochemical Society Transactions* 11, 575–586.
- Bray, E.E., Evans, E.D., 1961. Distribution of n-paraffins as a clue to recognition of source beds. *Geochimica et Cosmochimica Acta* 22, 2–15.
- Brocks, J.J., Summons, R.E., 2003. Sedimentary hydrocarbons, biomarkers for early life. In: Holland, H.D. (Ed.), *Treatise in Geochemistry*, 8, Elsevier, pp. 64–103.
- Burdige, D.J., 2006. *Geochemistry of Marine Sediments*. Princeton University Press, Princeton and Oxford.
- Capone, D.G., Burns, J.A., Montoya, J.P., Subramaniam, A., Mahaffey, C., Gunderson, T., Michaels, A.F., Carpenter, E.J., 2005. Nitrogen fixation by *Trichodesmium* spp.: an important source of new nitrogen to the tropical and subtropical North Atlantic Ocean. *Global Biogeochemical Cycles* 19, GB2024.
- Cecca, F., Pallini, G., Erba, E., Premoli-Silva, I., Coccioni, R., 1994. Hauterivian-Barremian chronostratigraphy based on ammonites, nannofossils, planktonic foraminifera and magnetic chronos from the Mediterranean domain. *Cretaceous Research* 15, 457–467.
- Channell, J.E.T., Erba, E., Muttoni, G., Tremolada, F., 2000. Early Cretaceous magnetic stratigraphy in the APICORE drill core and adjacent outcrop in Cismon (southern Alps Italy), and correlation to the proposed Barremian-Aptian boundary stratotype. *Geological Society of America Bulletin* 112, 1430–1443.
- Clift, P.D., 1992. The collision tectonics of the southern Greek Neotethys. *Geologische Rundschau* 81, 669–679.
- Cobianchi, M., Luciani, V., Menegatti, A., 1999. The Selli Level of the Gargano Promontory Apulia, southern Italy: Foraminiferal and calcareous nannofossil data. *Cretaceous Research* 20, 255–269.
- Coccioni, R., Premoli Silvá, I., Erba, E., 1992. Barremian-Aptian calcareous plankton biostratigraphy from the Gorgo Cerbara section (Marche, central Italy) and implications for plankton evolution. *Cretaceous Research* 13, 517–537.
- Comet, P.A., McEvoy, J., Brassell, S.C., Eglinton, G., Maxwell, J.R., Thomson, I.D., 1981. Lipids of an upper Albian limestone, Deep Sea Drilling Project Site 465, Section 465A-38-3. In: Thiede, J., Vallier, T.L. (Eds.), *Initial Reports DSDP* 62. Washington (U.S. Govt. Printing Office), pp. 923–937.
- Cranwell, P.A., 1973. Chain-length distribution of n-alkanes from lake sediments in relation to post-glacial environmental change. *Freshwater Biology* 3, 259–265.
- Danielian, T., Baudin, F., Gardin, S., Beltran, C., Masure, E., 2002. Early Aptian productivity increase as recorded in the Fourcade level of the Ionian zone of Greece. *Comptes Rendus de Geoscience* 334, 1087–1093.
- Danielian, T., Tsikos, H., Gardin, S., Baudin, F., Bellier, J.P., Emmanuel, L., 2004. Global and regional palaeoceanographic changes as recorded in the mid-Cretaceous (Aptian-Albian) sequence of the Ionian zone (NW Greece). *Journal of the Geological Society* 161, 703–709.
- Dédé, S., Cili, P., Bushi, E., Makbul, Y., 1976. Traits fondamentaux de la tectonique de Cukal. *Permbedjje Studimesh* 20/4, 15–33.
- Degnan, P.J., Robertson, A.H.F., 1998. Mesozoic-early Tertiary passive margin evolution of the Pindos Ocean (NW Peloponnese Greece). *Sedimentary Geology* 117, 33–70.
- Deres, F., Achérétéguy, J., 1980. Biostratigraphie des Nannoconides. *Bulletin des Centres de Recherches Exploration-Production Elf-Aquitaine* 4, 1–53.
- De Wever, P., 1976. Mise en évidence d'importants affleurements de roches éruptives à la base de la nappe du Pinde-Olones au sein de la 'Formation à Blocs' (Péloponnèse Grèce). *Annales de la Société Géologique du Nord* 97, 123–126.
- Didyk, B.M., Simoneit, B.R.T., Brassell, S.C., Eglinton, G., 1978. Organic geochemical indicators of palaeoenvironmental conditions of sedimentation. *Nature* 272, 216–222.
- Dumitrescu, M., Brassell, S.C., 2005. Biogeochemical assessment of sources of organic matter and paleoproductivity during the early Aptian Oceanic Anoxic Event at Shatsky Rise ODP Leg 198. *Organic Geochemistry* 36, 1002–1022.
- Dumitrescu, M., Brassell, S.C., Schouten, S., Hopmans, E.C., Sinninghe Damsté, J.S., 2006. Instability in tropical Pacific sea-surface temperatures during the early Aptian. *Geology* 34, 833–866.
- Dutta, S., Mallik, M., Kumar, K., Mann, U., Greenwood, P.F., 2011. Terpenoid composition and botanical affinity of Cretaceous resins from India and Myanmar. *International Journal of Coal Geology* 85, 49–55.
- Eglinton, G., Hamilton, R.J., 1967. Leaf epicuticular waxes. *Science* 156, 1322–1335.
- Erba, E., 1994. Nannofossils and superplumes: the early Aptian "nannoconid crisis". *Paleoceanography* 9, 483–501.
- Ensminger, A., 1977. Évolution de composés polycycliques sédimentaires. Ph.D. Thesis, University L. Pasteur, Strasbourg, 149 p. (Unpubl.).
- Erba, E., Channell, J.E.T., Claps, M., Jones, C., Larson, R.L., Opdyke, B., Premoli Silva, I., Riva, A., Salvini, G., Torricelli, S., 1999. Integrated stratigraphy of the Cismon APICORE (Southern Alps, Italy): a 'reference section' for the Barremian-Aptian interval at low latitudes. *Journal of Foraminiferal Research* 29, 371–391.
- Erba, E., 2004. Calcareous nannofossils and Mesozoic oceanic anoxic events. *Marine Micropaleontology* 52, 85–106.
- Erba, E., Duncan, R.A., Bottini, C., Tiraboschi, D., Weissert, H., Jenkyns, H.C., Malinverno, A., 2015. Environmental consequences of Ontong Java Plateau and Kerguelen Plateau volcanism. In: Neal, C.R., Sager, W.W., Sano, T., Erba, E. (Eds.), *The Origin, Evolution, and Environmental Impact of Oceanic Large Igneous Provinces*, 511, Geological Society of America, Special Paper, pp. 271–303.
- Erbacher, J., Thurow, J., Littke, R., 1996. Evolution patterns of radiolarian and organic matter variations: a new approach to identify sea-level changes in mid-Cretaceous pelagic environments. *Geology* 24, 499–502.
- Fleury, J.J., 1980. Les zones de Gavrovo-Tripoliza et du Pinde-Olones (Grèce continentale et Péloponèse du nord) Evolution d'une plate-forme et d'un bassin dans leur cadre alpin. *Société Géologique du Nord* 4, 1–473.
- Forster, A., Sturt, H., Meyers, P.A., Leg 207 Shipboard Scientific Party, 2004. In: Molecular biogeochemistry of Cretaceous black shales from the Demerara Rise: preliminary shipboard results from Sites 1257 and 1258 LEG 207, *Proceedings of the Ocean Drilling Program, Initial Reports Volume 207*.
- Godet, A., Föllmi, K., Bodin, S., de Kaenel, E., Matera, V., Adatte, T., 2010. Stratigraphic, sedimentological and palaeoenvironmental constraints on the rise of the Urgonian platform in the western Swiss Jura. *Sedimentology* 57, 1085–1128.
- Goldhaber, M.B., 2003. Sulfur-rich Sediments. In: Mackenzie, F.T., Holland, H.D., Turekian, K.K. (Eds.), *Treatise on Geochemistry, Sediments Diagenesis and Sedimentary Rocks*, 7, Elsevier, pp. 257–288.
- Greenwood, P.F., George, S.C., 1999. Mass spectral characteristics of C19 and C20 tricyclic terpanes detected in Latrobe Tasmanite oil shale. *European Journal of Mass Spectrometry* 5, 221–230.
- Greenwood, P.F., Arouri, K.R., George, S.C., 2000. Tricyclic terpenoid composition of Tasmanites kerogen as determined by pyrolysis GC-MS. *Geochimica et Cosmochimica Acta* 64, 1249–1263.
- Graziano, R., 2013. Sedimentology, biostratigraphy and event stratigraphy of the Early Aptian Oceanic Anoxic Event (OAE1a) in the Apulia Carbonate Platform Margin-Ionian Basin System (Gargano Promontory, southern Italy). *Cretaceous Research* 39, 78–111.

- Gröcke, D.R., Hesselbo, S.P., Jenkyns, H.C., 1999. Carbon-isotope composition of Lower Cretaceous fossil wood: ocean-atmosphere chemistry and relation to sea-level change. *Geology* 27, 155–158.
- Gröcke, D.R., 2002. The carbon isotope composition of ancient CO<sub>2</sub> based on higher plant organic matter. In: Gröcke, D.R., Kucera, M. (Eds.), *Understanding climate change: proxies, chronology, and ocean-atmosphere interactions*, 360, Royal Society, London, pp. 633–658.
- Herrle, J.O., Mutterlose, J., 2003. Calcareous nannofossils from the Aptian-lower Albian of southeast France: palaeoecological and biostratigraphic implications. *Cretaceous Research* 24, 1–22.
- Hinrichs, K.U., Summons, R.E., Orphan, V., Sylva, S.P., Hayes, J.M., 2000. Molecular and isotopic analysis of anaerobic methane-oxidizing communities in marine sediments. *Organic Geochemistry* 31, 1685–1701.
- Hochuli, P.A., Menegatti, A.P., Weissert, H., Riva, A., Erba, E., Premoli Silva, I., 1999. Episodes of high productivity and cooling in the early Aptian Alpine Tethys. *Geology* 27, 657–660.
- Hopmans, E.C., Schouten, S., Pancost, R.D., Van der Meer, M.T.J., Sinninghe Damsté, J.S., 2000. Analysis of intact tetraether lipids in archaeal cell material and sediments by high performance liquid chromatography/atmospheric pressure chemical ionization mass spectrometry. *Rapid Communications in Mass Spectrometry* 14, 585–589.
- Hu, X., Zhao, K., Yilmaz, I.O., Li, Y., 2012. Stratigraphic transition and palaeoenvironmental changes from the Aptian oceanic anoxic event 1a (OAE1a) to the oceanic red bed 1 (ORB1) in the Yenicesihlar section, central Turkey. *Cretaceous Research* 38, 40–51.
- Huck, S., Heimhofer, U., Rameil, N., Bodin, S., Immenhauser, A., 2011. Strontium and carbon-isotope chronostratigraphy of Barremian-Aptian shoal-water carbonates: Northern Tethyan platform drowning predates OAE 1a. *Earth and Planetary Science Letters* 304, 547–558.
- Jahren, A.H., Arens, N.C., Sarmiento, G., Guerrero, J., Amundson, R., 2001. Terrestrial record of methane hydrate dissociation in the Early Cretaceous. *Geology* 29, 159–162.
- Jenkyns, H.C., Wilson, P.A., 1999. Stratigraphy, paleoceanography, and evolution of Cretaceous Pacific guyots: relics from a greenhouse Earth. *American Journal of Science* 299, 341–392.
- Jenkyns, H.C., 2003. Evidence for rapid climate change in the Mesozoic-Paleogene greenhouse world. *Philosophical Transactions of the Royal Society of London, Series A* 361, 1885–1916.
- Jenkyns, H.C., 2010. Geochemistry of oceanic anoxic events. *Geochemistry, Geophysics, Geosystems* 11, Q03004.
- Karakitsios, V., 1995. The influence of preexisting structure and halokinesis on organic matter preservation and thrust system evolution in the Ionian basin, northwestern Greece. *AAPG Bulletin* 79, 960–980.
- Karakitsios, V., Tsikos, H., Agiadi-Katsiaouni, K., Dermitzoglou, S., Chatziharalampos, E., 2006. The use of carbon and oxygen stable isotopes in the study of global palaeoceanographic changes: examples from the Cretaceous sediment rocks of Western Greece. *Bulletin of the Geological Society of Greece* 39, 64–79.
- Karakitsios, V., Agiadi-Katsiaouni, K., 2007. Regional correlation and cyclostratigraphy in the mid-Cretaceous formations of the Ionian Zone. *Bulletin of the Geological Society of Greece* 40, 85–100.
- Karakitsios, V., 2013. Western Greece and Ionian Sea petroleum systems. *AAPG Bulletin* 97, 1567–1595.
- Kashiyama, Y., Ogawa, N.O., Kuroda, J., Shiro, M., Nomoto, S., Tada, R., Kitazato, H., Ohkouchi, N., 2008. Diazotrophic cyanobacteria as the major photoautotrophs during mid-Cretaceous oceanic anoxic events: Nitrogen and carbon isotopic evidence from sedimentary porphyrin. *Organic Geochemistry* 39, 532–549.
- Keller, C.E., Hochuli, P.A., Weissert, H., Bernasconi, S.M., Giorgioni, M., Garcia, T.I., 2011. A volcanically induced climate warming and floral change preceded the onset of OAE1a (Early Cretaceous). *Palaeogeography Palaeoclimatology Palaeoecology* 305, 43–49.
- Koopmans, M.P., Rijpstra, W.I.C., Klapwijk, M.M., de Leeuw, J.W., Lewan, M.D., Sinninghe Damsté, J.S., 1999. A thermal and chemical degradation approach to decipher pristane and phytane precursors in sedimentary organic matter. *Organic Geochemistry* 30, 1089–1104.
- Kuhnt, W., Holbourn, A., Moullade, M., 2011. Transient global cooling at the onset of early Aptian oceanic anoxic event (OAE) 1a. *Geology* 39, 323–326.
- Kuypers, M.M.M., Van Breugel, Y., Schouten, S., Erba, E., Sinninghe Damsté, J.S., 2004. N<sub>2</sub>-fixing cyanobacteria supplied nutrient N for Cretaceous oceanic anoxic events. *Geology* 32, 853–856.
- Lechner, M., Owens, J.D., Jenkyns, H.C., Lyons, T.W., Prosser, G., Parente, M., 2014. Sulphur isotopes indicate increased pyrite burial at the onset of OAE 1a in the Tethyan realm. *Geophysical Research Abstracts*, Vol. 16. EGU2014-11907, EGU General Assembly.
- Leckie, R.M., Bralower, T.J., Cashman, R., 2002. Oceanic anoxic events and plankton evolution: biotic response to tectonic forcing during the mid-Cretaceous. *Paleoceanography* 17, 13–29.
- Lee, C., Brocks, J.J., 2011. Identification of carotane breakdown products in the 1.64 billion year old Barney Creek Formation McArthur Basin, northern Australia. *Organic Geochemistry* 42, 425–430.
- Lefèvre, C., Cabanis, B., Ferrière, J., Thiebault, F., Platevoet, R., 1993. Mise en évidence d'une dualité dans le volcanisme triasique hellénique: apport de la géochimie des éléments traces. *Comptes Rendus de l'Académie des Sciences, Paris, Ser. II* 316, 1311–1318.
- Lozar, F., Tremolada, F., 2003. Calcareous nannofossil biostratigraphy of Cretaceous sediments recovered at ODP Site 1149 (Leg 185, Nadezhda Basin, western Pacific). In: Ludden, J.N., Plank, T., Escutia, C. (Eds.), *Proceedings ODP, Scientific Results*, 185, pp. 1–21.
- Luciani, V., Cobianchi, M., Jenkyns, H.C., 2001. Biotic and geochemical response to anoxic events: the Aptian pelagic succession of the Gargano Promontory (southern Italy). *Geological Magazine* 138, 277–298.
- Luciani, V., Cobianchi, M., Lupi, C., 2006. Regional record of a global oceanic anoxic event: OAE 1a on the Apulia Platform margin, Gargano Promontory, Southern Italy. *Cretaceous Research* 27, 754–772.
- Mackenzie, A.S., Patience, R.L., Maxwell, J.R., Vandebroucke, M., Durand, B., 1980. Molecular parameters of maturation in the Toarcian shales, Paris Basin France-I. Changes in the configurations of acyclic isoprenoid alkanes, steranes and triterpanes. *Geochimica et Cosmochimica Acta* 44, 1709–1721.
- Méhay, S., Keller, C., Bernasconi, S.M., Weissert, H., Erba, E., Bottini, C., Hochuli, P.A., 2009. A volcanic CO<sub>2</sub> pulse triggered the Cretaceous oceanic anoxic event 1a and a biocalcification crisis. *Geology* 37, 819–822.
- Menegatti, A.P., Weissert, H., Brown, R.S., Tyson, R.V., Farrimond, P., Strasser, A., Caron, M., 1998. High-resolution δ<sup>13</sup>C stratigraphy through the early Aptian "Livello Selli" of the Alpine Tethys. *Paleoceanography* 13, 530–545.
- Moldowan, J.M., Sundaraman, P., Schoell, M., 1986. Sensitivity of biomarker properties to depositional environment and/or source input in the lower Toarcian of S.W Germany. *Organic Geochemistry* 10, 915–926.
- Müller, G., Gastner, M., 1971. The "Karbonat-Bombe", a simple device for the determination of the carbonate content in sediments, soils and other materials. *Neues Jahrbuch für Mineralogie/Monatshefte* 10, 466–469.
- Mutterlose, J., Malkoč, M., Schouten, S., Sinninghe Damsté, J.S., Forster, A., 2010. TEX86 and stable δ<sup>18</sup>O paleothermometry of early Cretaceous sediments: Implications for belemnite ecology and paleotemperature proxy application. *Earth and Planetary Science Letters* 298, 286–298.
- Naafs, B.D.A., Castro, J.M., De Gea, G.A., Quijano, M.L., Schmidt, D.N., Pancost, R.D., 2016. Gradual and sustained carbon dioxide release during Aptian Oceanic Anoxic Event 1a. *Nature Geoscience* 9, 135–139.
- Naafs, B.D.A., Pancost, R.D., 2016. Sea-surface temperature evolution across Aptian Oceanic Anoxic Event 1a. *Geology* 44, 959–962.
- Najarro, M., Rosales, I., Moreno-Bedmar, J.A., de Gea, G.A., Barron, E., Company, M., Delanoy, G., 2011. High-resolution chemo- and biostrigraphic records of the early Aptian oceanic anoxic event in Cantabria (N Spain): palaeoceanographic and palaeoclimatic implications. *Palaeogeography Palaeoclimatology Palaeoecology* 299, 137–158.
- Neumann, P., Zacher, W., 2004. The Cretaceous sedimentary history of the Pindos Basin Greece. *International Journal of Earth Sciences* 93, 119–131.
- Okano, K., Sawada, K., Takashima, R., Nishi, H., Okada, H., 2007. Depositional environments revealed from biomarkers in sediments deposited during the mid-Cretaceous Oceanic Anoxic Events (OAEs) in the Vocontian Basin (SE France). In: Okada, H., Mawatari, S.F., Suzuki, N., Gautam, P. (Eds.), *Origin and Evolution of Natural Diversity. Proceedings of International Symposium "The Origin and Evolution of Natural Diversity"*, 1–5 October 2007. Sapporo, pp. 233–238.
- Palamakumbura, R.N., Robertson, A.H.F., Dixon, J.E., 2013. Geochemical, sedimentary and micropaleontological evidence for a late Maastrichtian oceanic seamount within the Pindos ocean (Arvi Unit S Crete, Greece). *Tectonophysics* 596, 250–262.
- Patruno, S., Triantaphyllou, M.V., Erba, E., Dimiza, M.D., Bottini, C., Kaminiski, M.A., 2015. The Barremian and Aptian stepwise development of the Oceanic Anoxic Event 1a (OAE 1a) crisis: integrated benthic and planktic high-resolution palaeoecology along the Gorgo a Cerbara stratotype section (Umbria–Marche Basin Italy). *Palaeogeography Palaeoclimatology Palaeoecology* 424, 147–182.
- Pedentchouk, N., Freeman, K.H., Harris, N.B., David, J., Clifford, D.J., Grice, K., 2004. Sources of alkylbenzenes in Lower Cretaceous lacustrine source rocks West African rift basins. *Organic Geochemistry* 35, 33–45.
- Pe-Piper, G., Hatzipanagiotou, K., 1993. Ophiolitic rocks of the Kerassies–Milia Belt, continental Greece. *Ophioliti* 18, 157–169.
- Pe-Piper, G., 1998. The nature of Triassic extension-related magmatism in Greece: evidence from Nd and Pb isotope geochemistry. *Geological Magazine* 135, 331–348.
- Peters, K.E., Moldowan, J.M., Schoell, M., Hempkins, W.B., 1986. Petroleum isotopic and biomarker composition related to source rock organic matter and depositional environment. *Organic Geochemistry* 10, 17–27.
- Peters, K.E., Walters, C.C., Moldowan, J.M., 2005. *The Biomarker Guide Volume 2: Biomarkers and Isotopes in Petroleum Exploration and Earth History*, 2nd ed. Cambridge University Press, 475–1155.
- Premoli-Silva, I., Erba, E., Salvini, G., Verga, D., Locatelli, C., 1999. Biotic changes in Cretaceous anoxic events. *Journal of Foraminiferal Research* 29, 352–370.
- Raiswell, R., Berner, R.A., 1985. Pyrite formation in euxinic and semi-euxinic environments. *American Journal of Science* 285, 710–724.
- Robertson, A.H.F., Karamata, S., 1994. The role of subduction-accretion processes in the tectonic evolution of the Mesozoic Tethys in Serbia. *Tectonophysics* 234, 73–94.
- Roth, P.H., 1978. Cretaceous nannoplankton biostratigraphy and oceanography of the northwestern Atlantic Ocean. *Initial Reports Deep Sea Drilling Project* 44, 731–760.
- Roth, P.H., 1983. Jurassic and Lower Cretaceous calcareous nannofossils in the western North Atlantic (Site 534): biostratigraphy, preservation, and some observations on biogeography and paleoceanography. *Initial Reports Deep Sea Drilling Project* 76, 587–621.

- Scalan, R.S., Smith, J.E., 1970. An improved measure of the odd-to-even predominance in the normal alkanes of sediment extracts and petroleum. *Geochimica et Cosmochimica Acta* 34, 611–620.
- Seifert, W.K., Moldowan, J.M., 1978. Applications of steranes, terpanes and monoaromatics to the maturation, migration and source of crude oils. *Geochimica et Cosmochimica Acta* 42, 77–95.
- Seifert, W.K., Moldowan, J.M., 1980. The effect of thermal stress on source-rock quality as measured by hopane stereochemistry. *Physics and Chemistry of the Earth* 12, 229–237.
- Simoneit, B.R.T., Sheng, G., Chen, X., Fu, J., Zhang, J., Xu, Y., 1991. Molecular marker study of extractable organic matter in aerosols from urban area of China. *Atmospheric Environment* 25A 2111–2129.
- Simoneit, B.R., Schoell, M., Dias, R.F., Aquino Neto, F.R., 1993. Unusual carbon isotope compositions of biomarker hydrocarbons in a Permian Tasmanite. *Geochimica et Cosmochimica Acta* 57, 380–383.
- Sinninghe Damst  , J.S., Kenig, E., Koopmans, M.P., Koster, J.G., Schouten, S., Hayes, J.M., De Leeuw, J.W., 1995. Evidence for gammacerane as an indicator of water column stratification. *Geochimica et Cosmochimica Acta* 59, 1895–1900.
- Sinninghe Damst  , J.S., Kuypers, M.M.M., Schouten, S., Schulte, S., Rulk  tter, J., 2003. The lycopane/C<sub>21</sub> n-alkane ratio as a proxy to assess palaeoxicity during sediment deposition. *Earth and Planetary Science Letters* 209, 215–226.
- Summons, R.E., Volkman, J., Boreham, C.J., 1987. Dinosterane and other steroid hydrocarbons of dinoflagellate origin in sediments and petroleum. *Geochimica et Cosmochimica Acta* 51, 3075–3082.
- Summons, R.E., Capon, R.J., 1988. Fossil steranes with unprecedented methylation in ring A. *Geochimica et Cosmochimica Acta* 52, 2733–2736.
- Summons, R.E., Jahnke, L.L., Hope, J.M., Logan, G.A., 1999. 2-Methylhopanoids as biomarkers for cyanobacterial oxygenic photosynthesis. *Nature* 400, 554–557.
- Tejada, M.L.G., Suzuki, K., Kuroda, J., Coccioni, R., Mahoney, J.J., Ohkouchi, N., Sakamoto, T., Tatsumi, Y., 2009. Ontong Java Plateau eruption as a trigger for the early Aptian oceanic anoxic event. *Geology* 37, 855–858.
- ten Haven, H.L., de Leeuw, J.W., Schenck, P.A., 1985. Organic geochemical studies of a Messinian evaporitic basin, northern Apennines (Italy) I: Hydrocarbon biological markers for a hypersaline environment. *Geochimica et Cosmochimica Acta* 49, 2181–2191.
- ten Haven, H.L., de Leeuw, J.W., Sinninghe-Damst  , J.S., Schenck, P.A., Palmer, S.E., Zumberge, J., 1988. Application of biological markers in the recognition of palaeo-hypersaline environments. *Lacustrine Petroleum Source Rocks*. Geological Society Special Publication, No. 40, Blackwell Scientific Publications, pp. 123–130.
- Thierstein, H.R., 1973. Lower Cretaceous calcareous nannoplankton biostratigraphy. *Abhandlungen der Geologischen Bundesanstalt* 29, 1–52.
- Thomas, J.B., Marshall, J., Mann, A.L., Summons, R.E., Maxwell, J.R., 1993. Dinosteranes (4,23,24-trimethylsteranes) and other biological markers in dinoflagellate-rich marine sediments of Rhaetian age. *Organic Geochemistry* 20, 91–104.
- Tissot, B., Pelet, R., Roucane, J., Combaz, A., 1977. Utilisation des alcanes comme fossiles g  ochimiques indicateurs des environnements g  ologiques. In: Campos, R., Goni, J. (Eds.), *Advances in Organic Geochemistry*, 1975. Empresa Nacional Adaro de Investigaciones Mineras Madrid (Espa  a) pp. 117–154.
- Tremolada, F., Erba, E., 2002. Morphometric analyses of Aptian *Assipetra infraretacea* and *Rucinolithus terebrodentarius* nannoliths: implications for taxonomy, biostratigraphy and paleoceanography. *Marine Micropaleontology* 44, 77–92.
- van Bentum, E.C., Reichart, G.-J., Sinninghe Damst  , J.S., 2012. Organic matter provenance, palaeoproductivity and bottom water anoxia during the Cenomanian/Turonian oceanic anoxic event in the Newfoundland Basin (northern proto North Atlantic Ocean). *Organic Geochemistry* 50, 11–18.
- van Breugel, Y., Schouten, S., Tsikos, H., Erba, E., Price, G.D., Sinninghe Damst  , J.S., 2007. Synchronous negative carbon isotope shifts in marine and terrestrial biomarkers at the onset of the Aptian oceanic anoxic event-1a: evidence for the release of methane into the atmosphere. *Paleoceanography* 22, PA1210.
- van Dongen, B.E., Roberts, A.P., Schouten, S., Jiang, W.-T., Florindo, F., Pancost, R.D., 2007. *Geochimica et Cosmochimica Acta* 71, 5155–5167.
- Volkman, J.K., Maxwell, J.R., 1986. Acyclic isoprenoids as biological markers. In: Johns, R.B. (Ed.), *Biological Markers in the Sedimentary Record*. Elsevier, Amsterdam, pp. 1–42.
- Volkman, J.K., Eglington, G., Corner, E.D.S., 1989. Sterols and fatty acids of the marine diatom *Biddulphia sinensis*. *Phytochemistry* 19, 1809–1813.
- Volkman, J.K., Rijpstra, W.I.C., de Leeuw, J.W., Mansour, M.P., Kackson, A.E., Blackburn, S.I., 1999. Sterols of four dinoflagellates from the genus *Protorcentrum*. *Phytochemistry* 42, 659–668.
- Wakeham, S.G., Freeman, K.H., Pease, T.K., Hayes, J.M., 1993. A photoautotrophic source for lycopane in marine water columns and sediments. *Geochimica et Cosmochimica Acta* 57, 159–165.
- Weissert, H., Lini, A., 1991. Ice age interludes during the time of Cretaceous greenhouse climate. In: M  ller, D.W., et al. (Eds.), *Controversies in modern geology*. Academic Press, London, pp. 173–191.
- Wilkin, R.T., Barnes, H.L., Brantley, S.L., 1996. The size distribution of frambooidal pyrite in modern sediments: An indicator of redox conditions. *Geochimica et Cosmochimica Acta* 60, 3897–3912.